Determining the Acoustic Mobility of Breast Cancer Cells

Author	Simon Olsson
Supervisor	Andreas Lenshof
Co-Supervisor	Tommaso De Marchi

Master´s Thesis in
Biomedical Engineering

LUNDS
UNIVERSITET

Faculty of Engineering LTH

Department of Biomedical Engineering

Lunds University

June 20, 2022

Abstract

Breast cancer is one of the most common forms of cancer detected in women. Its heterogeneity and large mutational landscape requires treatment strategies which varies between patients. Triple negative breast cancer (TNBC) is a particularly aggressive subtype which 12-17 % of breast cancer patient develop. It has no specific treatment and patients with TNBC generally has worse outcomes. To gain more knowledge about the disease, it is important to be able to isolate these cancer cells for down-stream analysis. We have used the novel microfluidic technique, acoustophoresis, as a method to separate the breast cancer cells. The samples that were used were frozen breast cancer tissue samples where cell suspension was obtained through cell dissociation and breast cancer cell lines MCF7, BT20 and BT549. The acoustic properties of the cancer cells suspended in PBS and PBS/Histopaque mixture were measured to design an optimised buffer solution which was then used for an attempt to improve separation. The patient samples turned out to be compromised when they were frozen down and therefore, viable cells could not be obtained. From the results of measuring the acoustic properties, PBS was the most optimum buffer out of the media which were tried, however, it was still not suitable for a good separation of the different cancer cells. In future studies, a larger range of density media should be tested to find a more suitable buffer media.

Acknowledgements

First of all, I would like to thank My P.Is Thomas Laurell and Emma Niméus for giving me the opportunity to work on this project. It has been a great learning experience with lots of challenges. I was able to overcome these challenges thanks to all the help I received from my wonderful supervisors and people from the lab. Andreas Lenshof, thank you for your supervision and always having a positive attitude despite all the troubles that I encountered during the thesis which was at some times quite a bit to deal with. Tommaso De Marchi, I cannot thank you enough for your assistance and guidance during the time I was totally lost and struggling with the tumor samples and the help you gave me with all the cancer related part of the project. Your feedback comments on my thesis drafts gave me a lot of good laugh, and it still does. Cecilia Magnusson, thank you for everything that you taught me about cell culturing and the times that you took care of my cell culture while I was absent due to sickness. You have been a real life saver. Lisa Rieckmann, thank you for all you've done for a smooth transition when handing over the project, and for the follow up Zoom meetings when I needed help. Thierry Baasch, thank you for explaining and helping me understand the parts of the theory that I had trouble understanding. Marc Isaksson, thank you for helping me make a really nice plot for the patient samples. Alexander Edthofer, thank you for helping me with the mobility measurement setup and always answering my questions when I was confused about the setup or the theory. Linda Péroux, thank you for your assistance with the acoustophoresis setup and helping me out with the cell culture. And big thanks to everyone that I had the pleasure of talking to, hanging out at the gym with and the after-work game nights/drink nights. You all made my stay at the BMC a great experience.

Lastly, I would like to thank my family and friends who supported me throughout the time I worked on the project with encouragements and kind words.

Contents

Chapter 1

Introduction

In this chapter, the background information necessary for the understanding of the thesis is presented, which includes basic information of the different types of breast cancer, microfluidics and the acoustofluidics. Finally, the goal of the thesis is stated.

1.1 The Breast

The prime function of the breast is the production, secretion, and ejection of milk [1]. Milk is produced by the mammary gland, which is comprised by two types of cells: luminal epithelial cells that produces milk, and the basal (and/or myoepithelial) cells which forms a mesh that surrounds the luminal epithelia and give it structure (basal laminae) figure 1.1. A basement membrane in turn surrounds the layer of myoepithelia and separates it from the stroma, which consists of connective tissue, fat tissue, blood vessels, nerves, and lymphatics [2].

1.2 Breast cancer

Breast cancer is one of the most common form of malignancy detected in women and is a heterogeneous disease with large mutational landscape [3]. The treatment strategies and treatment responses can therefore vary significantly among patients depending on tumor features [4]. Three markers are currently employed to classify breast cancer in the clinic: the estrogen receptor (ER), progesterone receptor (PgR), and the human epidermal growth factor receptor-2 (HER2) [5] [6]. Absence or

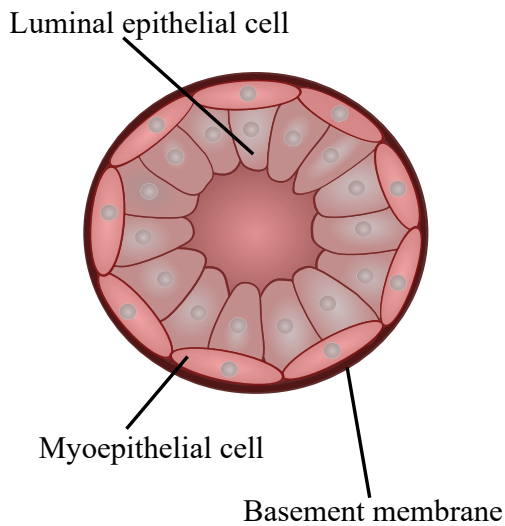

Figure 1.1: Illustration of the cross-section of the milk ducts in the breast. The luminal epithelia and myoepithelia cells and the surrounding basement membrane constructs the duct system in the breast.

presence of these receptors determine the type of breast cancer and the most appropriate treatment [7].

Hormone receptor positive breast cancer ER/PgR

Hormone receptor positive (HR^+) breast cancer is classified as expressing either ER and/or PgR, which are steroid hormone receptors involved in the expression of genes that play a crucial role in growth and survival of the cell. These receptors are expressed in 70 % of breast tumors [7] and, are treated with drugs that target and inhibit their function (endocrine therapy) [8] [9].

HER2 positive breast cancer

HER2 is a membrane bound receptor tyrosine kinase which act as a cancer driver by promoting cell proliferation, and inhibiting apoptosis [4]. HER2 positive breast tumors constitute 15-20 % of all breast cancer cases [10] and are generally treated with monoclonal antibodies and small molecule inhibitors [11] [12].

Triple negative breast cancer

Triple negative breast cancer (TNBC) is a particularly aggressive subtype of breast malignancy with generally worse outcomes in contrast to other types [13] [14]. Approximately 12-17 % of breast cancer patients develop TNBC, which is characterized by the lack of ER, PgR and HER2 expression. The likelihood of distant recurrence and death within a 5-year period is higher compared to other breast tumor types [14] [15]. The main treatment that is used is chemotherapy, which uses a combination of drugs that specifically target rapidly dividing cells, thus causing damage to tissues other than cancer [16].

TNBC is distinguished by the higher amount of tumor infiltrating lymphocytes (TILs) in the tumor micro-environment in comparison to other breast cancer types [15] [17]. Furthermore, the genomic instability of TNBC favors accumulation of somatic mutations, often leading to expression of neoantigens [17]. With the discovery of this unique micro-environment and the neoantigens, new approaches of targeted treatment in the context of immunotherapy are being developed [17].

1.3 Immune cells in breast tissues

The presence of immune cells indicates an inherent protective role of the immune system which is important during normal breast development and maturation [4].

Most immune cells derive from myeloid (monocytes, macrophages, dendritic cells) or lymphoid (T lymphocytes and B lymphocytes) lineages in the bone marrow and have a constant presence among breast lobules. More specifically, the immune cells that are found are $CD8^+$, $CD11c^+$, $CD45^+$, $CD68^+$ and with lower densities $CD4^+$ and $CD20^+$ [18].

Tumor infiltrating lymphocytes

Tumor infiltrating lymphocytes (TILs) are immune cells that have infiltrated a specific tissue to target cancer cells. Their presence is important due to their influence in tumor progression, response to immunotherapy, and predicting treatment response and outcomes [19].

$CD8^+$ T lymphocytes

$CD8^+$ cytotoxic T lymphocytes interacts with antigens to destroy foreign pathogens. $CD8^+$ T cells destroys the tumor cells, when detected, through direct or indirect cell lysis, the latter through production of cytokines [20].

$CD4^+$ T lymphocytes

$CD4^+$ effector and $CD4^+$ regulatory T cells affect the regulation of host immune response against cancer and other diseases in distinct ways. $CD4^+$ effector T lymphocytes play an important role in priming and maintenance of $CD8^+$ and shown to be required for subsequent expansion of memory $CD8^+$T cells. $CD4^+$ regulatory T lymphocytes in contrary, have an immunosuppressive function. By inhibiting the function of other leukocytes by either interacting directly, or indirectly through secreting anti-inflammatory molecules [21], $CD4^+$ regulatory cells maintain self-tolerance and prevent autoimmune responses [22].

$FOXP3^+$ T regulatory lymphocytes

Forkhead box 3 ($FOXP3^+$) T regulatory (Treg) lymphocytes are $CD4^+$ T cells that express the FOXP3 gene. FOXP3 regulates Treg cell generation and its expression is induced when a naive $CD4^+$ T cell is activated [19]. As a regulatory T lymphocyte, $FOXP3^+$ down regulate the immune response induced by $CD8^+$ T lymphocytes. [23]. In the light of this discovery, the $CD8^+$/$FOXP3^+$ ratio could be useful for clinical prognostics [19].

Cancer Immunotherapy

Cancer immunotherapy is a treatment that use primed immune cells to target and destroy the tumor. Adoptive cell therapy (ACT) is one of the most common immune therapy approaches which employs autologous or allogenic immune cells that are administered to the patient after priming (activation of immune cells by presenting antigens to increase immune response) and expansion (increase in number). Recently, it has been suggested to expand the use of TILs based ACT to other malignancies such as breast cancer [24]. In the light of this, the development of protocols to isolate tumor cells and TILs can become important for future research in cancer treatment.

1.4 Microfluidics

When fluids are confined to small volumes such as microchannels, their behavior is altered compared to when they are present in the macro-scale. Microfluidics is the field that study and utilize this behavior.

Laminar flow

In a microchannel, fluid flow is laminar, which is deterministic and thus allows for mathematical modelling of the flow patterns and concentrations 1.2. There are several useful non-dimensional numbers that can be used to predict the behavior of a fluid in a system.

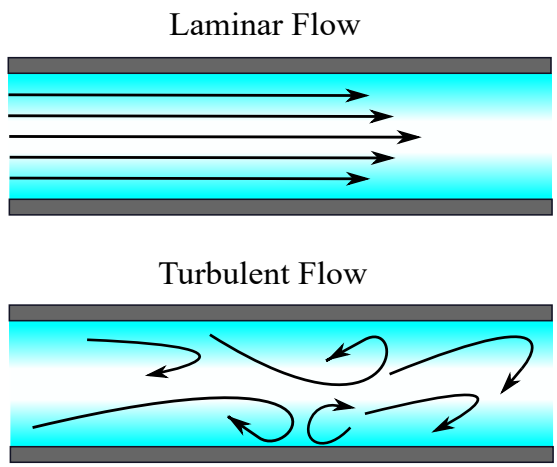

Figure 1.2: Flow of liquids in microchannels are laminar, which allows for mathematical modelling of migration of particles suspended in the fluid due to its deterministic nature. Turbulent flow is in contrast difficult to model with all the swirls which causes high rate of mixing.

$$Re = \frac{\rho u L}{\mu} \tag{1.1}$$

Reynolds number as shown in Equation 1.1, is used to predict whether the flow in the system is laminar or turbulent.ρ is the density of the fluid, u is the average flow

speed of the fluid in the system, L is the characteristic length of the system and μ is the viscosity of the fluid. Typically, if the $Re < 2000$, the flow is laminar and in microchannels Re is usually less than 1 [25].

$$Pe = \frac{uL}{D} \tag{1.2}$$

The Péclet number in Equation 1.2 is useful in predicting whether convection or diffusion is the dominant force of transport of particles or fluid in the system where D is the diffusion coefficient [25].

Parabolic flow profile

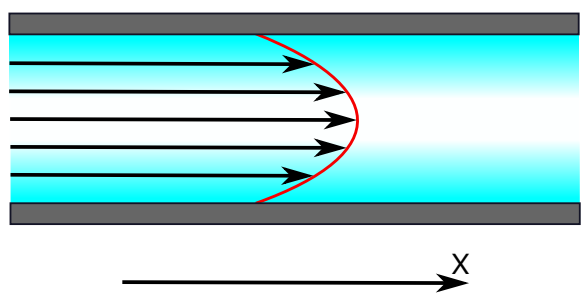

Figure 1.3: Illustration of the flow profile within a microfluidic channel. The flow has a parabolic shape due to friction at the wall slowing the velocity of the fluid close to the wall.

The general differential equation called the Navier-Stokes equation describes the flow of any fluid within a channel of any shape. The set of Equation 1.3 and 1.4 are simpler solution of the Navier-Stokes when the fluid is Newtonian fluid and certain boundary condition such as the no-slip condition is applied [25].

$$0 = -\frac{\partial p}{\partial x} + \eta \frac{\partial^2 u_x}{\partial y^2} + \frac{\partial^2 u_x}{\partial z^2} \tag{1.3}$$

$$0 = \frac{\partial p}{\partial y} = \frac{\partial p}{\partial z} \tag{1.4}$$

Equation 1.4 indicates that there are no pressure gradient in the y or z direction where all flow runs parallel to x and the flow becomes parabolic as seen in figure 1.3 [25].

Stokes drag

A particle in motion within a viscous medium will be subjected to a frictional force termed Stokes drag in the opposite direction to the movement.

$$\mathbf{F}_{\mathbf{drag}} = -6\pi\eta a v \tag{1.5}$$

Stokes drag for a spherical particle is described by Equation 1.5 where η is the dynamic viscosity of the medium and v is the velocity of the particle.

1.5 Acoustophoresis

Particles suspended in a medium in a microfluidic device can be manipulated using acoustic waves. The technique, termed acoustophoresis, utilizes the acoustic radiation forces and streaming forces that arise from the ultra sound standing waves to move the suspended particles relative to the surrounding medium [26]. Due to the flow within microfluidic channels being laminar, it is possible to separate and sort particles/cells within the channel in a predictable and controlled manner. Acoustophoresis has further advantages such as continuous mode of operation and gentle handling of sensitive biological samples [27].

Standing waves in microchannels

Sound is oscillation in pressure that propagates through a medium such as gases, liquids or solids. In liquids, sound propagates as compression waves which compress and expand the medium as it travels. When two sound waves meet, they each contribute to the total pressure through interference. If the sound waves have the same frequency and amplitude, constructive interference occur which give rise to a standing wave. In a micro channel, the propagating wave is reflected against the channel wall which allows for standing waves to form. By creating microfluidic channels with dimensions which are integer multiple of half the wavelength, acoustic resonance can be generated. The resonance will give rise to pressure nodes and anti-nodes at exact locations in the channel depending on the wavelength.

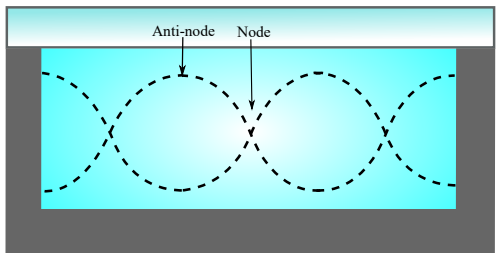

Figure 1.4: Illustration of the standing waves forming in a cross section of a micro channel with nodes and anti-nodes forming at specific distances in the channel which is half the wavelength.

Primary acoustic radiation force

Acoustic radiation force F_{rad} is the force that acts on a particle, which can be micro-beads, cells or bacteria, along the acoustic pressure gradient when subjected to a resonant acoustic pressure field p_1 [28]. The force arises from the acoustic waves scattering on the suspended particles which causes a transfer of momentum to the particles. This result in migration of the suspended particles relative to the surrounding medium [26]. In one dimension, the pressure field and the acoustic radiation force can be expressed as:

$$p_1 = p_a \cos(k_y y) \tag{1.6}$$

$$\mathbf{F}_{rad} = 4\pi\phi a^3 k_y E_{ac} \sin(2k_y y) e_y \tag{1.7}$$

p_1 is the first order pressure field of amplitude p_a, $k_y = 2\pi/\lambda$ is the wave number, ϕ is the acoustic contrast factor, E_{ac} is the acoustic energy density, a is the particle radius.

$$\phi = \frac{f_1}{3} + \frac{f_2}{2} = \frac{1-\tilde{k}}{3} + \frac{\tilde{\rho}-1}{2\tilde{\rho}+1} = \frac{1}{3}\left(\frac{5\tilde{\rho}-2}{2\tilde{\rho}+1} - \tilde{\kappa}\right) \tag{1.8}$$

The acoustic contrast factor ϕ, describes the ratio of density and compressibility of the particle in relation to the surrounding medium. f_1 is the factor dependent on the compressibility of the particle κ_p in relation to compressibility of the medium

κ_m where $f_1 = 1 - \tilde{\kappa}$ and $\tilde{\kappa} = \frac{\kappa_p}{\kappa_m}$ and f_2 is the factor dependent on the density of the particle ρ_p in relation to density of the medium ρ_m where $f_2 = \frac{2(\tilde{\rho}-1)}{2\tilde{\rho}+1}$ and $\tilde{\rho} = \frac{\rho_p}{\rho_m}$ [27]. The sign of the radiation force is determined by the material properties of the particle/cell relative to the medium they are suspended in. The contrast factor reveal whether the particle will move towards the pressure node or the anti-node of the standing wave in the channel [28] [29]. If ϕ>0 the particle migrate towards the nodes and if ϕ<0, it migrates towards the anti-nodes [30]. The Equation 1.9

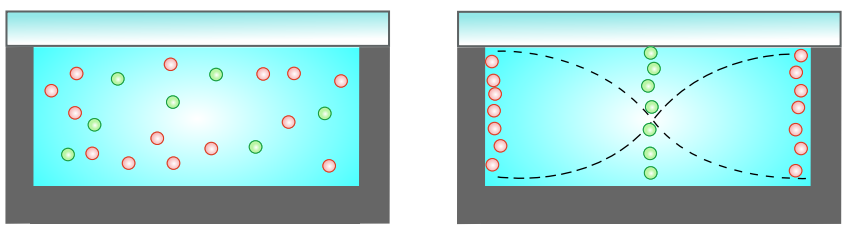

Figure 1.5: Illustration of a mixture of two types of particles with contrast factors of opposite sign being separated by acoustophoresis. The left image is when ultrasound is not yet applied and the right image is when ultrasound is applied. Particles with ϕ>0 migrates to the node and particles with ϕ<0 to the anti-nodes of the standing wave.

describes the total acoustic energy within a channel and is termed acoustic energy density.

$$E_{ac} = \frac{p_a^2 \kappa_0}{4} \tag{1.9}$$

By combining the equations for acoustic radiation force Equation 1.7 and the stokes drag Equation 1.5, we get Equation 1.10 for the velocity of the particle in the acoustic standing wave [31]:

$$v_y = \frac{2}{3\eta}\phi(\tilde{\kappa}, \tilde{\rho}) k a^2 E_{ac} \sin(2ky) \tag{1.10}$$

Secondary acoustic radiation force

Secondary acoustic radiation force is the acoustically induced inter-particle effect caused by sound waves scattering off from one particle to another. This effect

becomes more significant as the distances between particles becomes smaller than two particle diameter [26]. Equation1.11 describes the secondary acoustic radiation force.

$$F_{sec} = 4\pi a^6 \frac{(\rho_p - \rho_m)^2(3\cos^2\theta - 1)}{6\rho_m d^4} v(x) - \frac{\omega^2 \rho_m (\kappa_p - \kappa_m)^2}{9d^2} p^2(x) \tag{1.11}$$

d is the center to center distance between the particles [32].

Acoustic streaming

Acoustic streaming is flow that originates from acoustic waves that travels through a liquid medium. It is caused by either viscous attenuation of the acoustic waves in the fluid or by boundary interactions with the walls of the container [33]. In acoustofluidic devices, these streaming often occur in the bulk fluid or in the viscous boundary layers near solid walls [26]. For particles with diameters below 1 µm, the viscous drag force from acoustic streaming is the dominant force. This is due to primary acoustic radiation force on these particles is weak because it scales with the volume of the particles [34].

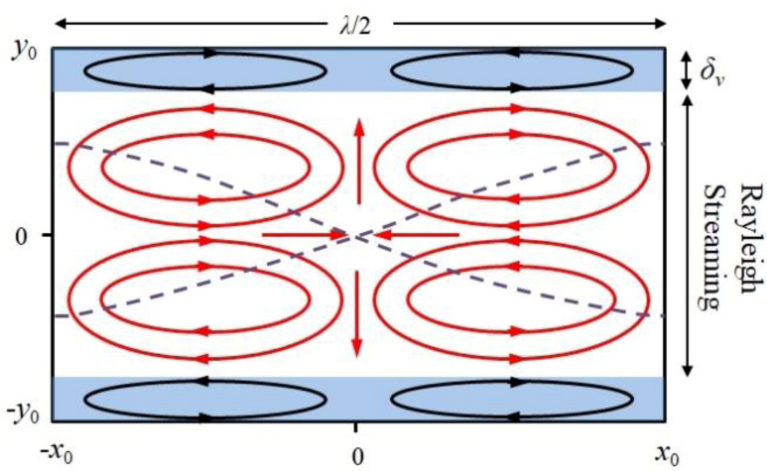

Figure 1.6: Illustration of the acoustic streaming phenomenon in an acoustic microfludic system. The flow in red are the vortices termed Rayleigh streaming due to them being first described by Lord Rayleigh [35]. Reproduced with permission from Taylor & Francis from reference [35]

. .

1.6 Aim of the thesis

The goal of this project is the following:

1. Optimize the tumor cell dissociation protocol
2. Catalogue the acoustic mobility of different tumor cell lines
3. Show proof of concept of improved separation with optimized buffer solution
4. Show proof of concept that it is possible to distinguish different cancer cell types by acoustic mobility
5. Perform acoustophoretic separation of dissociated tissue

Chapter 2

Material and Methods

In this chapter, the methods and materials used during the project is described. This includes the process of culturing and preparing the control cell line, analysing the tumor tissue for cell dissociation through histochemistry, acquiring tumor cell suspension through cell dissociation, and the separation of the tumor cell suspension with acoustophoresis.

2.1 Control cell line

The control cell lines that was cultured for this project are following: MCF7, BT20 and BT549 which are breast cancer cell lines. MCF7 is an ER/PGR positive breast cancer, which is an invasive carcinoma of no special type (NST) which is the most common type of breast cancer [36] [37]. BT20 is an invasive ductal carcinoma and of the TNBC subtype [37]. BT549 is of the papillary invasive ductal carcinoma (PIDC) and of the TNBC subtype [37].

2.2 Taking cell lines into culture

The cell line stocks are stored at -80°C in 1.5 mL cryovials and thawed in the 37°C water bath. The cell suspension and 19 mL of supplemented RPMI 1640 cell medium which is pre-warmed to 37°C is added to a T75 cell culture flask (Sigma Aldrich). The cell medium is supplemented with 50 mL of heat inactivated fetal bovine serum (HI-FBS), 2.5 mL of 10 mg/mL Gentamicin, and 6 mL of Pen/Strep. The cell line is incubated for 24 hours in the incubator at 37°C and 5 % CO_2 and the medium is

changed. The cells are incubated at 37°C, 5 % CO_2 until confluent and the medium is changed every 2 or 3 days.

2.3 Splitting cells

The medium is aspirated and the flask is rinsed with phosphate buffered saline (PBS) pre-warmed to 37°C. The PBS is aspirated after the rinse and 1 mL of trypsin pre-warmed to 37°C is added, and the flask is placed in the incubator for 6-10 min. If the cells have been released into suspension and no major conglomerate is formed, 9 mL of pre-warmed RPMI 1640 cell medium is added. The content is pipetted up and down to break off remaining cell-cell junctions to obtain single cell suspension which is transferred to a 15 mL Falcon tube. The suspension is centrifuged for 5 min at 500g, 4°C and the supernatant is removed. The cells are suspended in pre-heated cell medium and 10 µL is pipetted to a 1 mL vial and stained using 10 µL trypan blue to be counted in the cell counter.

Appropriate fraction is transferred to a T75 cell culture flask and pre-heated cell medium is added to reach 20 mL total volume. The flask is then placed in the incubator.

2.4 Taking cells to experiment

During the splitting of cells, after the cells are counted, the amount corresponding to 10^6 cells per vial used for experiment is transferred to a 15 mL falcon tube and centrifuged for 5 min at 500g at 4°C. The supernatant is aspirated and the cells are resuspended and divided into equal aliquots and placed on ice.

2.5 Evaluation of tumor cell content with histochemistry

In order to determine the tumor cell content of the biopsy samples, H&E-staining must be performed. For that, the tissue sample must be cut in 10 µm thin slides through cryosection. Leica CM1950 cryostat (Leica Biosystems) was used to cut the tumor tissue samples in thin slides which was placed on a microscopy slide. The cut tissue was then stained with Mayers Hematoxylin and Eosin staining. Hematoxylin stains the cell nucleus in purple color and eosin, which is the name of a group

of fluorescent acidic compound, is used to stain the stroma. The precise washing procedure is described below:

1. dH_2O 5min
2. Mayers Hematoxylin 10 min
3. Tap H_2O 10 min
4. Eosin (Erythrosin) 3 min
5. dH_2O 1 min Dipping
6. Ethanol 95% 1 min Dipping
7. Ethanol 100% 5 min
8. Xylene 2x5 min
9. Mount slides with pertex

The slides were then observed under the microscope to verify whether the tissue sample had enough tumor cells to be used in the experiment. The qualitative evaluation was based on the ratio between total tumor cell area and the total area of the cut tissue. Samples yielding more than 50 % tumor cell area were recommended to use in the cell dissociation experiment.

2.6 Cell dissociation

To obtain single cell suspension of the patient tumor tissue, the tumor cells were dissociated through mechanical and enzymatic digestion by using gentleMACS™Octo Dissociator (Miltenyi) shown in figure 2.1. 100-200 mg of tissue sample cut up into 2 mm pieces were added to the C-tubes (Miltenyi). Enzyme mix solution from the Tumor dissociation kit, human (Miltenyi) was added to the tubes containing the tissue samples. Lastly, 2 % final concentration FBS and 0,5 % final concentration Bovine serum albumin (BSA) was added to the tubes. The reason of addition of the BSA is to lower the amount of free fatty acid (FFA) in the mixture due to FFA being suggested that it acts as an unspecific enzyme inhibitor [38]. The addition of BSA which has been shown to have FFA binding property could potentially lower the enzyme inhibiting effect of the FFA [39]. The tubes with the samples were placed on

Figure 2.1: Miltenyis gentleMACS™Octo dissociator which was used to dissociate the tumor tissue sample for separation with acoustophoresis. Image taken from miltenyibiotec.com

the gentleMACS™Octo Dissociator (Miltenyi) and the 37C_h_TDK_2 program was then ran on the gentleMACS™Octo Dissociator(Miltenyi). After the mechanical and enzymatic digestion was completed, the cell suspension was strained through cell strainers with mesh size of 70 µm into a 50 mL Falcon tube. 20 mL of RPMI 1640 was added to the strainer and the obtained cell suspension was centrifuged at 500g for 5 min. All but 2 mL of supernatant was removed and the cells were resuspended and transferred to FACS tubes, ready for staining and subsequent flow cytometry analysis.

2.7 Staining and flow cytometry analysis

The cells were stained with anti-EpCAM (Epithelial Cell Adhesion Molecule) antibody-PE (BD), Anti-CD324-APC (Miltenyi), AnnexinV-FITC (Miltenyi) and with DAPI (Miltenyi). EpCAM antibody binds to the epithelial adhesive molecule which is a known tumor marker on the cell surface of basal type tumor. CD324 also known as E-Cadherine is a surface molecule present on tumor cells of the luminal type. AnnexinV stains apoptotic cells and cell debris. It binds to a lipid present on the inner layer of the lipid bi-layer of the cells which becomes accessible on apoptotic cells and cell debris. DAPI stains the cell nucleus by binding to DNA. The stained cells are analyzed using flow cytometry seen in figure 2.2.

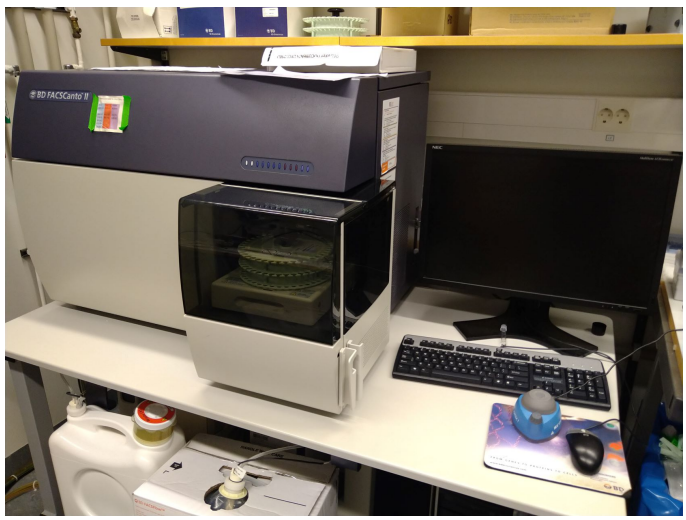

Figure 2.2: Fluorescence Activated Cell Sorting used to analyse the stained tumor samples.

2.8 Acoustic Mobility measurement

To find out the density and compressibility of an particle, the acoustic mobility and contrast factor of the suspended particles needs to be measured. For this, the setup shown in figure 2.3 was used. The acoustofluidic chip shown in figure 2.4 is equipped with two transducers which is set on 2 MHz and 5 MHz respectively.

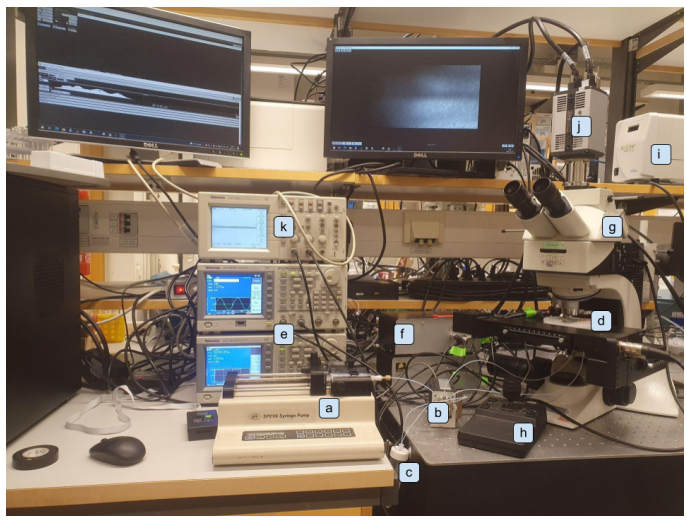

Figure 2.3: Mobility measurement setup used for the experiments. The components that comprise the setup are: a) Syringe pump b) Multi port valve c) Waste holder d) Microfluidic chip e) Signal generators f) Signal amplifiers g) Microscope h) Joystick table controller i) X-Cite 120Q light source j) Andor sCMOS camera k) Oscilloscope

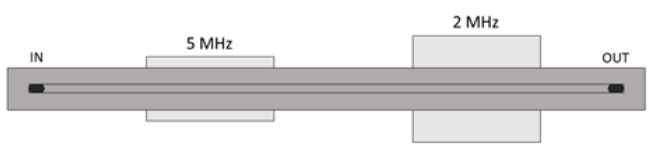

Figure 2.4: Illustration of the microfluidic chip used for mobility measurement. It is equipped with two transducers to generate 2 MHz and 5 MHz frequency respectively.

The particles are first vertically focused using the 5 MHz transducer which will force the particles to migrate into a single plane which is perpendicular to the separator. Then the vertically focused particles are focused horizontally towards the horizontal node with a second transducer at 2 MHz as illustrated in figure 2.5. The motion of the particles during vertical focusing is recorded using a Particle tracking software called GDPTLab, shown in figure 2.6, to calculate their velocities at different positions.

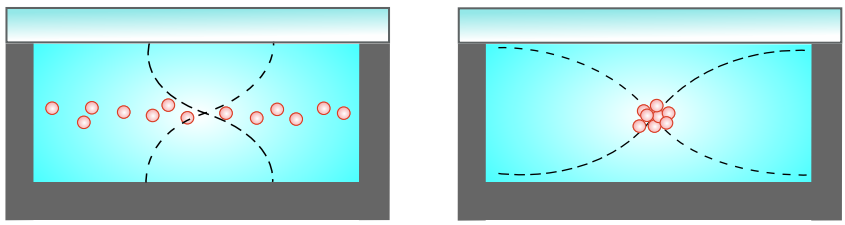

Figure 2.5: Illustration of the two step process of mobility measurement. First the particles are vertically focused with the 5 MHz transducer shown in the left image and then the particles are focused horizontally focused while measuring the migration with particle tracking software.

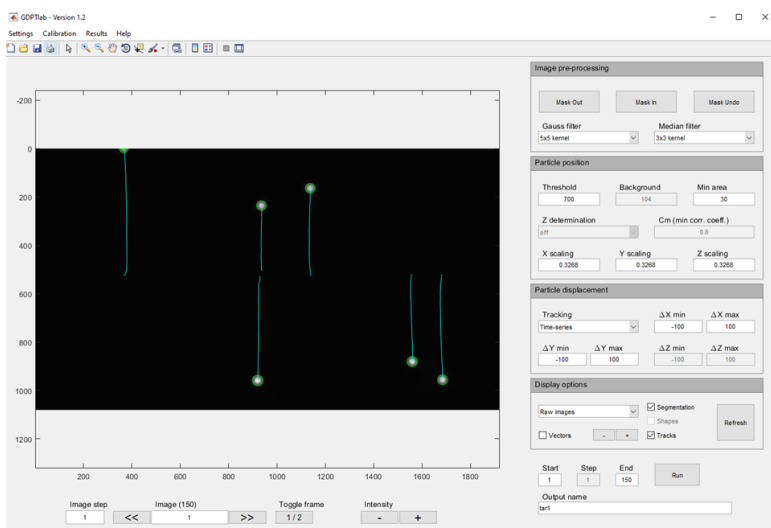

Figure 2.6: The trajectories of the particles were analyzed using the particle tracking software GDPTLab.

To obtain the contrast factor of a particle with unknown density and compressibility, we first need to find out the acoustic energy density of the channel using a reference particle with known contrast factor. The length of the channel that the measurement is done on is 600 µm and the MATLAB script divides this up in

twelve 50 µm long slices. The position of the particles and their velocity within the slices is used to create a curve fit seen in figure 2.7.

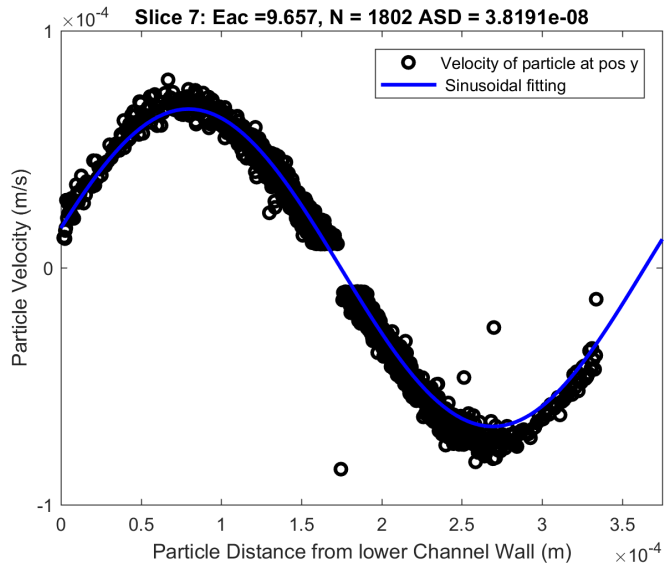

Figure 2.7: A curve fit of velocity measurements of reference beads. By measuring the speed of a reference particle with known size, density and compressibility, which travels within an acoustic field, we can use this curve fit to calculate the acoustic energy density within the channel. The acoustic energy density value is then used for contrast factor calculation of particles with unknown density and compressibility.

The amplitude of the curve and the wavelength corresponds to the term in front of the sinus function and the wave number in equation 1.10 which can be written as,

$$v_y = \alpha \sin(\beta y) \tag{2.1}$$

where the fitted parameter corresponds to the theory where,

$$\alpha = \phi a^2 k \frac{2}{3\eta} E_{ac}, \qquad \beta = 2k \tag{2.2}$$

By rearranging the equation 2.2, it gives us the acoustic energy density of the channel for each of the twelve slices which accounts for the variation of its strength within the channel.

$$E_{ac} = \frac{3\eta\alpha}{2ka^2\phi} \tag{2.3}$$

To calculate the contrast factor of the cells with unknown contrast factor, we use the ratio between α_p of the reference particle and the α_c of the cell,

$$\frac{\alpha_p}{\alpha_c} = \frac{\phi_p a_p^2 k \frac{2}{3\eta} E_{ac}}{\phi_c a_c^2 k \frac{2}{3\eta} E_{ac}} = \frac{\phi_p a_p^2}{\phi_c a_c^2} \tag{2.4}$$

which then gives us,

$$\phi_c = \frac{\alpha_c}{\alpha_p} \frac{\phi_p a_p^2}{a_c^2} \tag{2.5}$$

By measuring the contrast factor in two different medium which has different density and compressibility, ρ_1, ρ_2 and κ_1, κ_2, the compressibility and the density of the cells can be calculated. Because the contrast factor depends on the relative density and compressibility of the particle and the medium, we can setup the following equation to solve for the cells density and compressibility.

$$\phi_1 = \frac{1}{3}\left(\frac{5\tilde{\rho_1} - 2}{2\tilde{\rho_1} + 1} - \tilde{\kappa_1}\right) \tag{2.6}$$

$$3\phi_1(2\rho_c/\rho_1 + 1) = (5\rho_p/\rho_1 - 2) - \kappa_p/\kappa_1(2\rho_p/\rho_1 + 1) \tag{2.7}$$

$$-\kappa_p(2\rho_p/+\rho_1) = \rho_p(6\phi_1\kappa_1 - 5\kappa_1) + 2\kappa_1\rho_1 + 3\phi 1\kappa_1\rho_1 \tag{2.8}$$

We then define

$$a_1 = (6\phi_1\kappa_1 - 5\kappa_1), b_1 = 2\kappa_1\rho_1 + 3\phi 1\kappa_1\rho_1, c_1 = 2, d_1 = \rho_1 \tag{2.9}$$

$$a_2 = (6\phi_2\kappa_2 - 5\kappa_2), b_2 = 2\kappa_2\rho_2 + 3\phi 2\kappa_2\rho_2, c_2 = 2, d_2 = \rho_2 \tag{2.10}$$

by isolating κ_p we get

$$(c_2\rho_p + d_2)(a_1\rho_p + b_1) = (C_1\rho_p + d_1)(a_2\rho_p + b_2) \tag{2.11}$$

$$a_1c_2\rho_p^2 + \rho_p(b_1c_2 + a_1d_2) + b_1d_2 = a_2c_1\rho_p^2 + \rho_p(b_2c_1 + a_2d_1) + b_2d_1 \tag{2.12}$$

$$0 = (a_1c_2 - a_2c_1)\rho_p^2 + (b_1c_2 + a_1d_2 - b_2c_1 - a_2d_1)\rho_p + b_1d_2 - b_2d_1 \tag{2.13}$$

Here we define,

$$\alpha = (a_1c_2 - a_2c_1), \beta = (b_1c_2 + a_1d_2 - b_2c_1 - a_2d_1), \gamma = b_1d_2 - b_2d_1 \tag{2.14}$$

and at last we get,

$$\alpha\rho_p^2 + \beta\rho_p + \gamma = 0 \tag{2.15}$$

$$\rho_p = \frac{-\beta \pm \sqrt{\beta^2 + 4\alpha\gamma}}{2\alpha} \tag{2.16}$$

With equation 2.16 the density of the object is calculated and the compressibility can now be known.

The medium that has been used was Histopaque and a mixture of 50 % PBS and 50 % Histopaque. The density of the Histopaque and the histopaque/PBS mixture was measured with Density and sound velocity meter DSA 5000 M (Anton Paar) shown in figure 2.8.

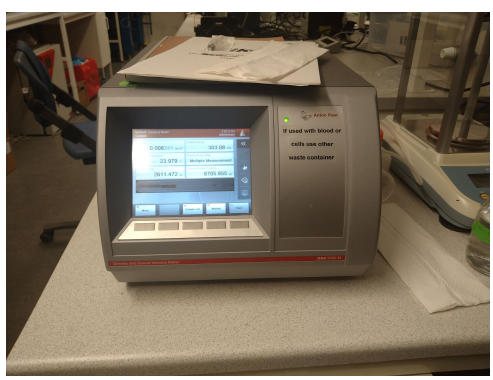

Figure 2.8: The Density and sound velocity meter DSA 5000 M from Anton Paar used to measure the densities of the mediums used in the experiments.

Measurement on reference fluorescence beads

The beads that were used were 4.99 µm red fluorescence beads which was used as reference for the calculation of the contrast factor for the cells. The samples were prepared by adding 5 µL of 2.5 % w/v fluorescence beads to 3 mL of buffer solution which was vortexed and loaded on the setup.

Measurement on tumor cells

Initially, the tumor cells were stained with anti-EpCAM antibodiy coupled with FITC to enable it for detection in the fluorescence microscope. After further experimentation, the cells were instead stained with Calcein AM (Thermo Fisher) which is a cell-permeant dye that stains live cells. The dye can permeate the cell membrane which is then modified within to a structure which is retained within the cell. The intracellular esterase activity of live cells further convert the non-fluorescent calcein AM into a fluorescent dye [40]. The cells were stained in the following procedure: 20 µL of 1 mM Calcein AM stock solution was added to 10 mL of PBS buffer to create a 2 µM Calcein AM working solution. The harvested cells are centrifuged and washed with PBS and the working solution is applied directly to the cells to obtain the final concentration of 10^6 cells/mL. The resuspended cells are then incubated in dark at 37°C for 40 min.

2.9 Size measurement of cells

Figure 2.9: The Amnis ImagestreamX-MKII which was used to measure the size of the tumor cells

To calculate the acoustic contrast factor, the size of the cells must be known. With the Imagestream X - MKII, shown in figure 2.9, an imaging flow cytometer from Amnis Corporation, the size of the cells were measured. The flow cytometer takes an image of the cells that can be used to measure its length and obtain information of the size distribution in the sample.

2.10 Separation of cancer cells

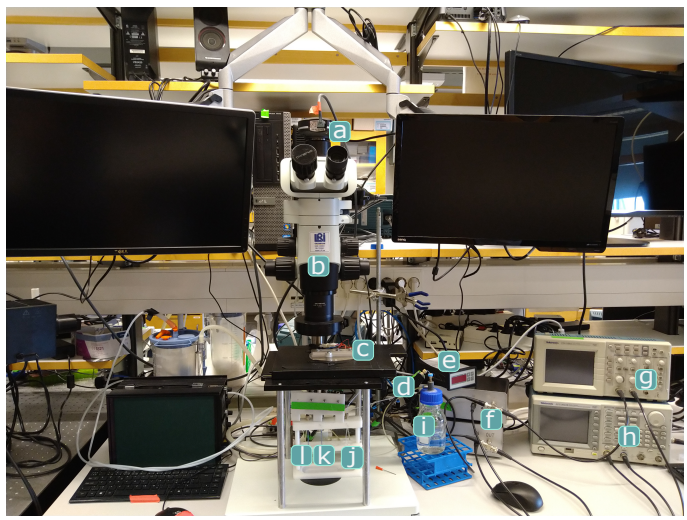

Figure 2.10: Acoustophoresis setup used for the experiments. The components that comprise the setup are: a) The camera b) Microscope c) The acoustophoresis chip d) Flow sensor e) Temperature controller f) Signal amplifiers g) Oscilloscope h) Signal generator i) Center buffer j) Sample inlet k) Center outlet l) Side outlet

The separation of the cancer cells is performed in the acoustophoresis setup illustrated and described in figures 2.10 and 2.11. The acoustophoresis chip has two transducers. One at 5 MHz which is placed in the pre-focusing region and one with 2 MHz at the separation region. The dimension of the channel at the pre-focusing region allows for simultaneous lateral and vertical focusing when the ultrasound is applied. The pre-focusing confines the suspended objects in a predisposed position within the channel. Due to the boundary conditions and parabolic flow profile, the velocity of the objects depends on the position within the channel as seen in figure 2.12, however, the pre-focusing will circumvent this issue by controlling the objects starting position when they enter the separation channel.

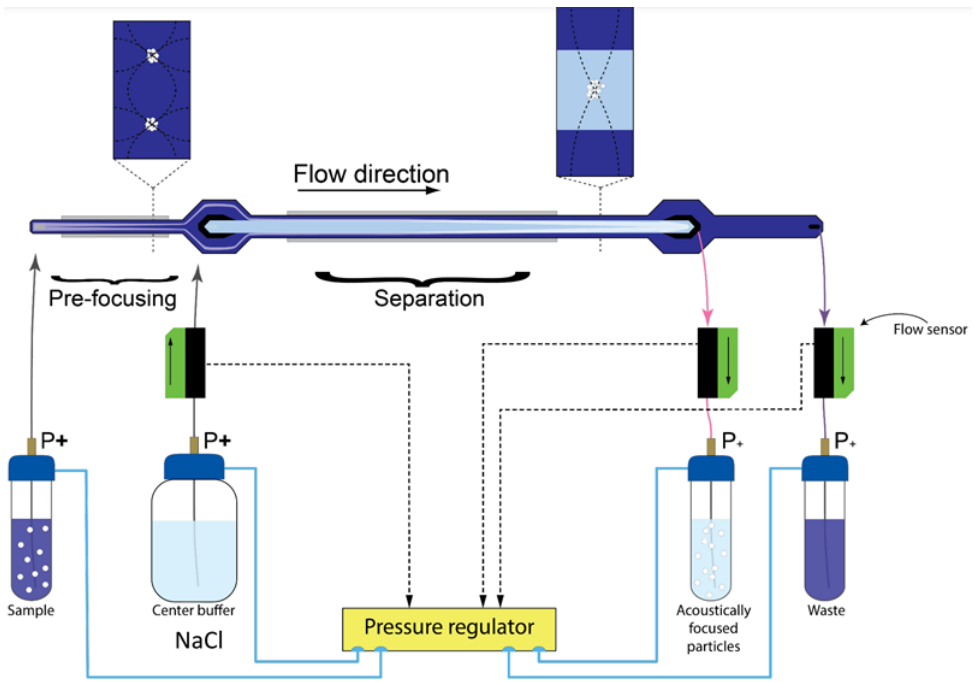

Figure 2.11: Schematic of the acoustophoresis setup. The particles and cells are pre-focused in the pre-focusing region to ensure them having the same starting point. This allows a more controlled migration when they are being focused in the separation region of the channel. The content of the center buffer is changed accordingly to what is being tested in the experiment. Image taken from [41].

The separation is done in two different media. One is PBS and the other is the optimised medium which is made using the density and compressibility data of the cancer cells from the acoustic mobility measurement experiment that will be separated. Two different cell lines will be separated in the experiment. The harvested cells is stained with the Calcein AM Green and Calcein AM Red-Orange respectively as described in the mobility measurement experiment. 1 mL of each cell suspension that has been diluted to 1/3 was added to a FACS tube and was loaded onto the setup.

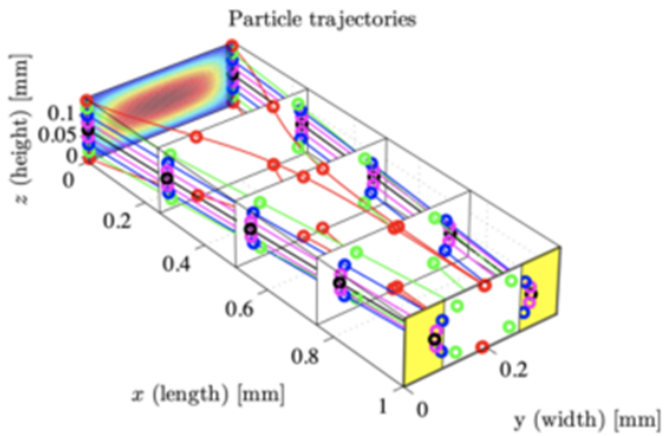

Figure 2.12: Depending on the position of the particles and cells, they will travel at different velocity along the length of the channel. The position of the suspended particles and cells will affect the retention time and thus the time spent in the acoustic field. Image from [42]

The flow rate was set to 150 µL /min with the side inlet ratio of 25 % and side outlet ratio of 75 %. This is to push the cells towards the side in the pre-focusing part of the channel. This setting will give the cells long time and the maximum distance of travel, which will give better separation. The focusing voltage was the variable that was changed to find the optimum separation of the cells. The range of voltage to test is first determined by finding the voltage that causes all cells to exit the side outlet and another voltage that focus all the cells to the center outlet. When the range is defined, it was step wise divided into the voltages that was going to be tested. The fractions that was collected from each voltage step is then analysed with the flow cytometer to determine the efficiency and the purity of separation. The following equations are used to calculate the efficiency and the purity of the separation,

$$Separation\ efficiency = \frac{n_{1,center}}{n_{1,center} + n_{1,side}} \tag{2.17}$$

$$Separation\ purity = \frac{n_{1,center}}{n_{1,center} + n_{2,center}} \tag{2.18}$$

where n_{center} is the number of cells that has been collected in the center outlet and n_{side} is the number of cells that has been collected in the side outlet.

Chapter 3

Results and Discussion

In this chapter, the results from the experiments are presented and discussed in the following order: Evaluation of tumor cell content, cell dissociation, separation of tumor cells with acoustophoresis.

3.1 Evaluation of tumor cell content

Through qualitative analysis, the tumor cell content in 14 samples have been evaluated through H&E-staining seen in figure 3.1 and 3.2. The tumor slice in figure 3.1(a) we have a higher tumor cell and lower stroma content compared to slice in figure 3.1(b). Furthermore we can see a net-like structure in the center left part in figure 3.1(a), which has likely been fat cells which has been dissolved during the H&E-staining procedure when dipped in ethanol. The results indicates that samples are of heterogeneous character where tumor cell content can vary between different pieces from the same sample. The process of evaluation was conducted to determine which samples have a potential to give high yield of tumor cells when they undergo the cell dissociation process. For each sample, the tumor cell content value was pooled and the tumor samples which contained more than 50 % were selected for the cell dissociation experiment.

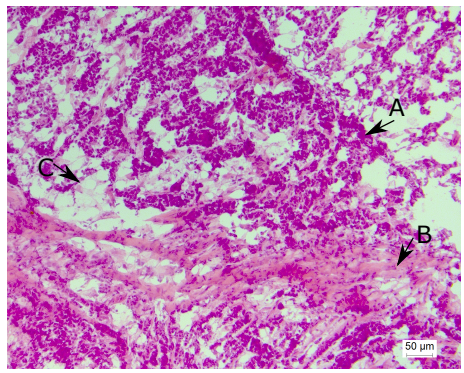

(a)

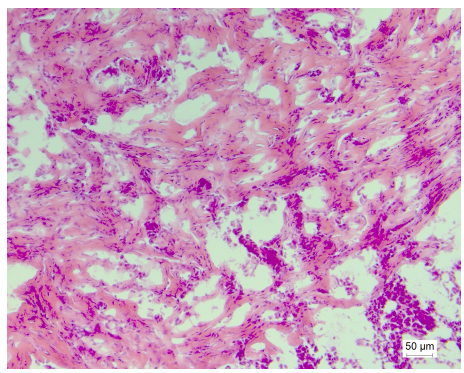

(b)

Figure 3.1: The cryosected and stained tumor tissue samples observed under a microscope to estimate the tumor cell content. The nucleus of the cells are colored in purple (A) and the stroma is colored in pink (B) from H&E-staining. The fat cells (C) appears as a net-like structure due to them being dissolved when dipped in ethanol during the staining process. Both images are taken from the same sample but of different cuts and it shows that the amount of tumor cell, fat cell and stroma differs substantially between the cuts even though they are from the same sample.

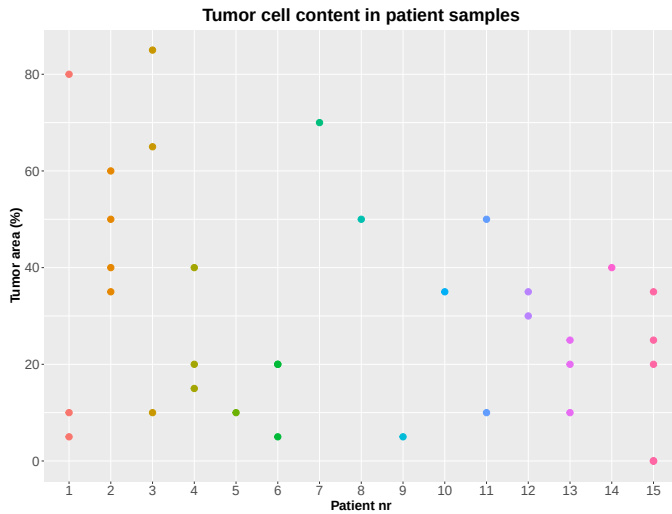

Figure 3.2: Estimation of the percentage of the tumor slice area consisting of tumor cells. Each dot represents a slice from the tumor tissue. 1-4 slices were evaluated from each patient sample depending on the size and number of pieces the tissue has been cut up into at the pathology department.

3.2 Cell dissociation

During the course of the project, there was only one successful attempt of cell dissociation and the the results from that attempt is presented in figure 3.3. In the side scatter vs forward scatter plot, all the registered counts are concentrated on the lower end of the forward scatter axis. Forward scatter axis represents the size of the particle, where lower intensity correspond with smaller particle. Side scatter corresponds with the complexity or granularity of the cells. Compared to the results from the MCF7 control cell line presented in figure 3.4, the size of the read outs of tumor tissue samples are smaller which could indicate that the cells have ruptured and reduced to fragments. The results from the rest of the control and tumor samples are presented in table 3.1. The control cell line result shows that the staining procedure worked. However, there are very low live cell count in the tumor samples. Furthermore, the EpCAM positivity and E-Cadherin positivity within the gating is consistently very low in the samples, which indicates that there are barely any tumor cells present in the suspension. This result was

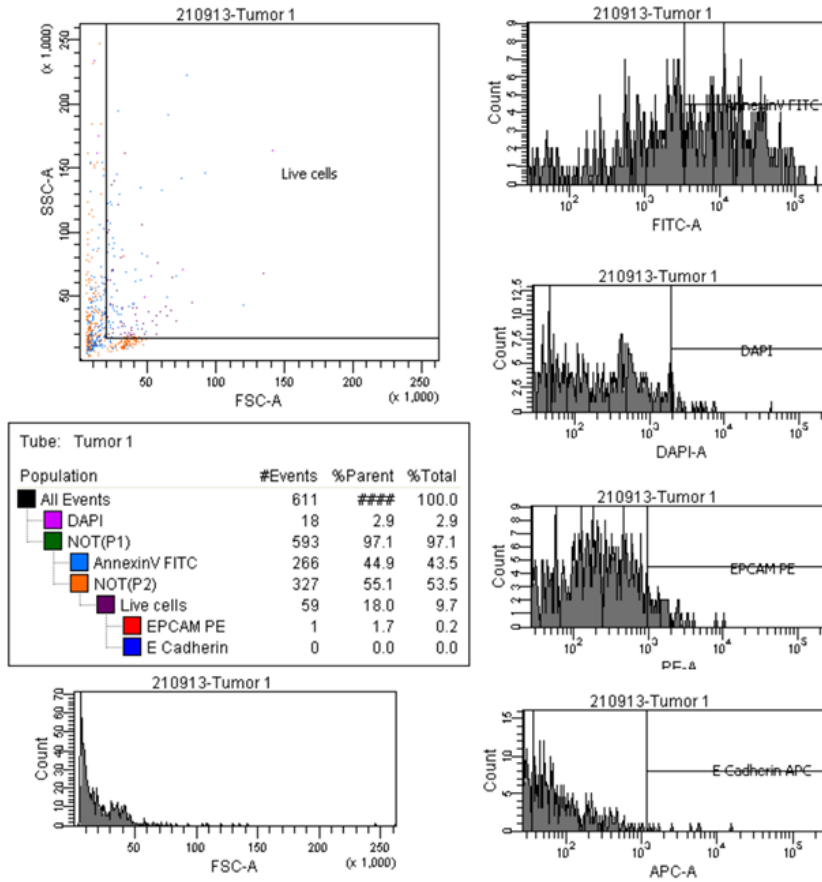

Figure 3.3: FACS analysis of the tumor tissue sample with very generous gating settings. The gate settings are defined to find out how many of the live cells are tumor cells. This is done by first excluding all the dead cells which is stained with either DAPI and/or AnnexinV-FITC. Then, the tumor cells, which are stained with EpCAM PE and/or E-Cadherin APC, are sorted out from the events within the live cell gating. There is a high count of AnnexinV FITC positive events which indicates that we have a lot of dead/apoptotic cells. Furthermore, the count for EpCAM and E-Cadherin postive events are very low whithin the gating which means, there is not much cancer cells in the cell suspension.

Table 3.1: Results from a cell dissociation and staining experiment. The amount of live cells is in general less than 20 % of the total events recorded for the tumor samples and the amount of EpCAM and E-Cadherin positivity is around 2 % or less. The live cell percentage in the AnnexinV control is 1.9 % because the cells were killed to act as control for AnnexinV which binds to dead cells and cell fragments.

Sample	% Live Cells	% DAPI+	% AnnexV+	% EpCAM+	% E-Cad+
MCF7 Unstained	90	0.2	0.1	0	0
MCF7 EpCAM control	85.5	5.9	0	53.3	0
MCF7 DAPI control	76	14.9	0	0	0
MCF7 AnnexV control	1.9	0.9	75.1	0	0.1
BT20 E-Cad control	98	0.2	0.2	0	90.2
Tumor sample 1	9.7	2.9	43.5	0.2	0
Tumor sample 2	15.1	3.6	28.8	0.2	2.3
Tumor sample 3	10.2	1.9	36.6	0.7	0
Tumor sample 4	3.9	2.8	61	0	0
Tumor sample 5	8.9	0.5	24.8	0	0
Tumor sample 6	19.5	0.5	14.9	0.5	0.7
Tumor sample 7	18.1	1	34.6	1.1	0.5
Tumor sample 8	17.6	0.7	33.3	1.6	2.1

also seen in previous experiments done within the group. The conclusion that is derived from observing these results is that there is very low potential of obtaining cell suspension with sufficient tumor cell content on which the acoustophoresis separation experiment can be performed on. One reason for the low tumor cell

content could be due to tissue samples which has been given by the pathology department at MAS doesn't contain a lot of tumor cells. This is due to most of the tissue has been used for diagnostics and the experiments had to be done on the left over material.

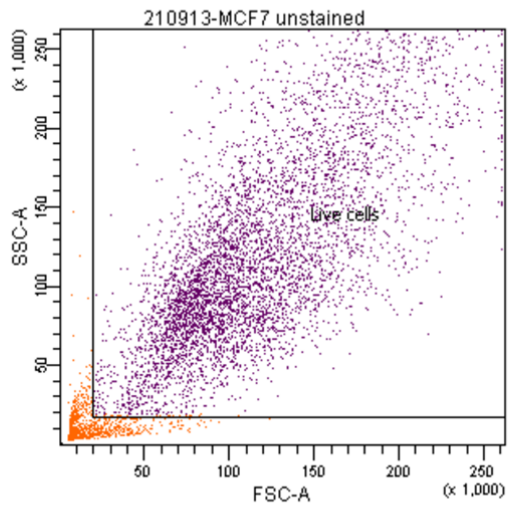

Figure 3.4: Scatter plot of the unstained MCF7 control cell line obtained from FACS analysis. Live cells are marked in purple within the gating and the dead cells which are outside of the gating are colored in orange.

Furthermore, by analyzing the results, there was a suspicion that tumor cells within the tumor tissue sample could be compromised even before being used in the experiment. This could be due to the tissue samples not been frozen using any sort of cryo-preservation protocol at the pathology department. To confirm this, the control cell lines were frozen in a similar manner to the tumor samples and then analysed with FACS. The result is shown in figure 3.5 which confirms the hypothesis that the freezing of tumor samples without any specific freezing protocol lead to cell death. The scope of the thesis had to be changed due to this result because not enough live cells could be extracted from the frozen tumor tissue samples to perform acoustophoresis experiment. If fresh tumor tissues could be obtained, it might have resulted in higher viable cell yield which was seen in one of the result from previous study within the group.

(a)

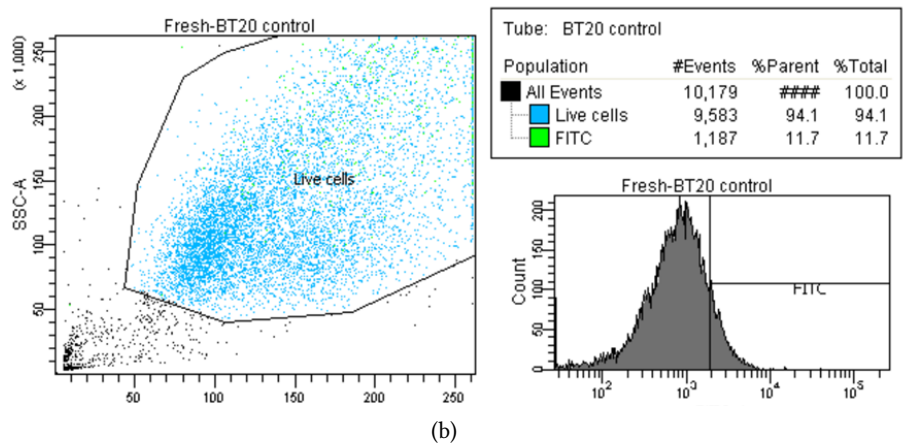

(b)

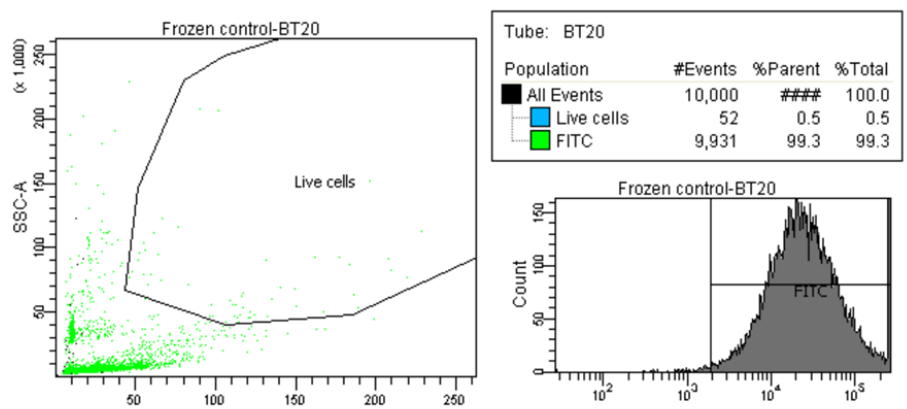

Figure 3.5: a) The control cell line BT20 used as control for E-cadherine staining for one of the cell dissociation experiment which is used here for comparison to the frozen BT20 cell lines. The majority of the counts are within the gating for live cells and FITC-positivity is at 11.7 % which indicates that we have around 90 % viable cells. b) The BT20 cell line that has been frozen in the -80 °C freezer which has been thawed, stained with PE, APC, DAPI and FITC staining. The result of the PE, APC and DAPI staining is not shown here. There is less than 1 % of cells within the live cells gating and nearly 100 % FITC-positivity which suggests that the freezing without any cryopreservation procedure is detrimental for the survival of cells.

3.3 Size measurement of the cells

In figures 3.6-3.8 the results from the cell measuring using the ImagestreamX is presented. The gating is setup to exclude unwanted events such as clusters of cells, cell debris, and reference beads. In the BT549 measurement, there was a separate population consisting of smaller cells and beads in the BT549 sample. The smaller cells has minimum overlap in size compared to the bigger population. The population which consists of cells in the range of 20-30 µm with median size of 23.5 µm is the most interesting population. In the BT20 population, there is a larger spread in the size of the cells compared to the other cell lines where the largest cell that was observed had a length of 43.5 µm while the average cell had a length of around 22 µm.

As seen in the results presented above, there are variation in size of the cells and due to the radius of the cells having a significant effect on its velocity, we will most likely see a distribution in the contrast factor of the cells which could become a problem when determining the optimum buffer solution.

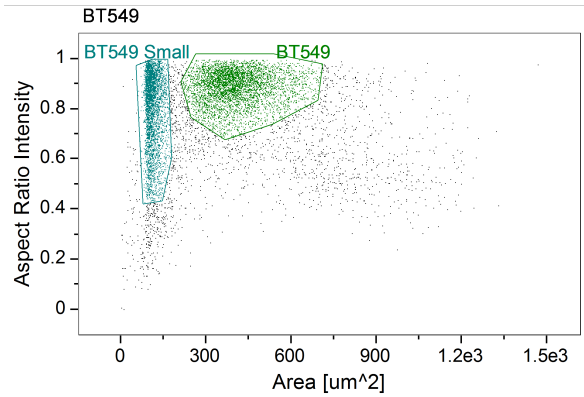

Area [um^2], Aspect Ratio Intensity

Population	Count	%Gated
All	10000	100
BT549	4592	45.9
BT549 Small	3621	36.2

(a)

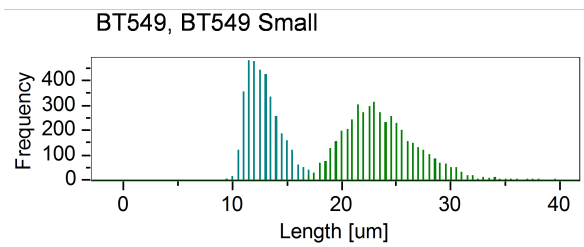

Length [um]

Population	Count	Mean	Median	Std. Dev.
BT549	4592	23.84	23.5	4.399
BT549 Small	3621	13.22	12.5	3.39

(b)

Figure 3.6: a) Scatter plot of the imaged BT549 cells with area on the x-axis. The gating is set up to exclude clusters and debris. b) Size distribution of the cells within the gating. The cells are around roughly 24 µm in diameter.

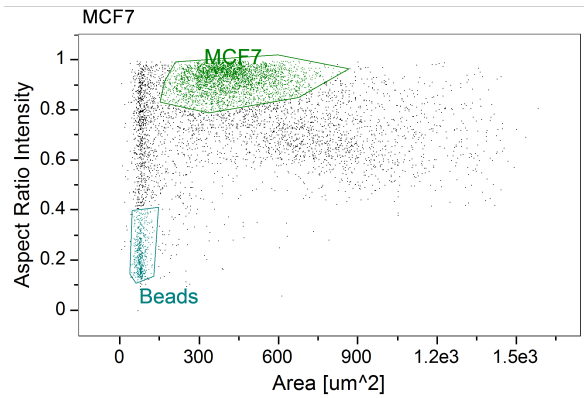

Area [um^2], Aspect Ratio Intensity

Population	Count	%Gated
All	6855	100
MCF7	3264	47.6
Beads	509	7.43

(a)

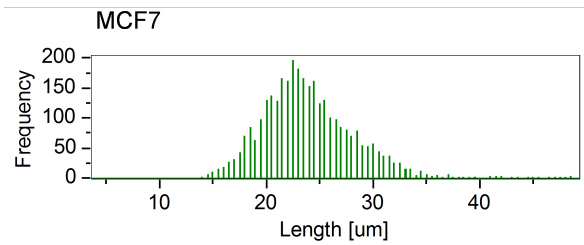

Length [um]

Population	Count	Mean	Median	Std. Dev.
MCF7	3264	24.42	23.5	6.447

(b)

Figure 3.7: a) Scatter plot of the imaged MCF7 cells with area on the x-axis. The gating is set up to exclude clusters and debris. b) Size distribution of the cells within the gating. The cells are around roughly 22 µm in diameter.

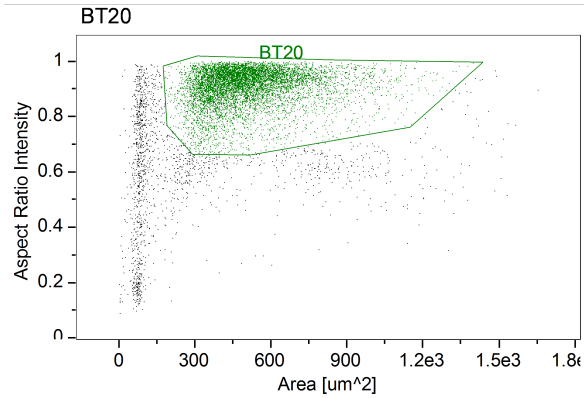

Area [um^2], Aspect Ratio Intensity

Population	Count	%Gated
All	10000	100
BT20	8409	84.1

(a)

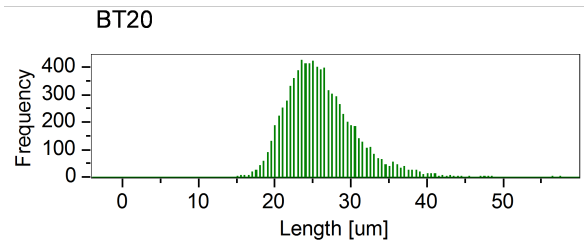

Length [um]

Population	Count	Mean	Median	Std. Dev.
BT20	8409	26.21	25.5	5.858

(b)

Figure 3.8: a) Scatter plot of the imaged cells with area on the x-axis. The gating is set up to exclude clusters and debris. b) The size distribution of the BT20 cell line within the gate. We have cells from the range of 18 µm to 40 µm with mean value 26.21 µm.

3.4 Acoustic mobility measurement of the cells

The cells that have been stained with anti-EpCAM FITC were not visible in the setup which made it unable to record the migration of the cells. The cells could be vaguely seen in the setup when the filter was switched to dark field (DF) which confirmed that the problem wasn't the absence of cells. By analysing the sample with FACS, it was verified that the staining was successful due to them being detectable in the FACS. The stained cells were also observed on another fluorescence microscope which showed that the cells were visible. however only faintly. These result leads to a hypothesis that the camera used in the mobility measurement setup could be not sensitive enough to observe the cells stained with anti-EpCAM FITC antibodies.

In subsequent experiments, staining with Calcein AM was tested which was believed to give stronger fluorescence signal. It did give a stronger signal as expected, however, the signal was still not strong enough for the cells to be clearly visible in the setup for mobility measurement. In the other setup, the cells were clearly visible and giving a strong signal as shown in figure 3.9. The problem that needed to be addressed was figuring out which part of the microscope of the mobility measurement setup was the cause of the problem of detecting the cells.

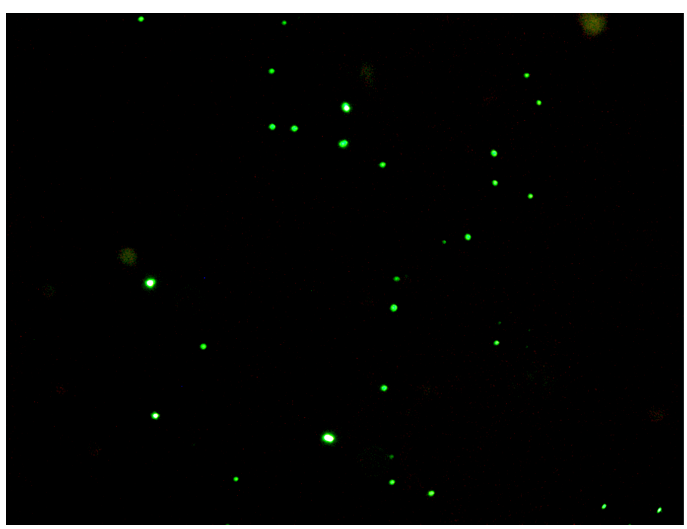

Figure 3.9: The MCF7 cell line that has been stained with Calcein AM observed under the separation setup. It gives stronger signal than the anti-EpCAM FITC staining. Therefore it became the staining of choice in the experiments that followed.

When the optic cables were exchanged between the mobility setup and the separation setup, the cells stained with Calcein AM were finally visible as seen in figure 3.10. It turned out that it was the optic cable used in the mobility setup that was defective which made it unable to observe the cells.

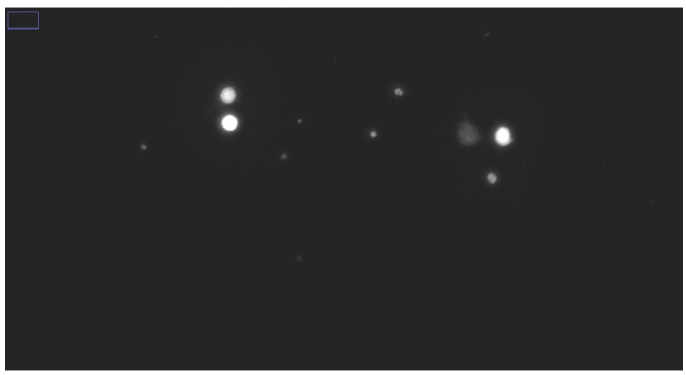

Figure 3.10: The BT549 cell line that has been stained with Calcein AM observed in the mobility measurement setup.

The cells were first levitated with the 5 MHz frequency, then the 2 MHz frequency was applied to focus them to the center. The image taken during the levitation and focusing steps are presented in figure 3.11. In table 3.2 the result of the contrast factor calculation is presented. The median length of the cell was used for the

Table 3.2: The results of the contrast factor measurement of the breast cancer cell lines suspended in PBS. The contrast factor values presented under each experiment are the mean value of all the slices from that experiment. For the calculation the median length was used.

		Exp 1	Exp 2	Exp 3		
Cell line	E_{ac}	ϕ	ϕ	ϕ	Mean	SD
BT549	17.7032	0.0063	0.0095	0.0089	0.0090	0.0019
BT20	15.2246	0.0042	0.0040	0.0053	0.0044	0.0009
MCF7	11,8609	0,0089	0,0086	0,0104	0,0093	0,0008

calculation. The contrast factor is quite small which is reasonable due to cells consists mostly of water. However, BT20 appears to have smaller value than the two other cell lines that has been measured. BT549 and MCF7 seems to have similar

value on the contrast factor which could pose a challenge to design a buffer to separate them.

(a)

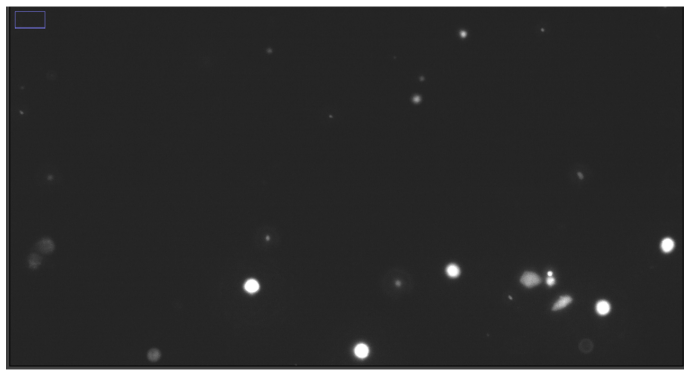

(b)

Figure 3.11: BT549 cell line that has been stained with Calcein AM in the acoustic mobility measurement setup. a) The cells are levitated with the 5 MHz frequency. b) Cells are focused to the center with the 2 MHz frequency. Their migration is measured to calculate the acoustic mobility.

To obtain the density and mobility of the cells, we did another set of measurements using a different media. BT549, was suspended in Histopaque and BT20 was suspended in 50 % V/V Histopaque and PBS which the density and sound velocity is presented in table 3.3.

With the values from table 3.3, and the Equation 2.16 in the methods section, the

density and the compressibility was calculated which is shown in table 3.4.

Table 3.3: The measured density and the sound velocity of the different buffer medium that was used in the measurement of acoustic mobility of the cancer cell lines. The measurements were done using the Density and sound velocity meter DSA 5000 M from Anton Paar. The measured density and sound velocity is when the medium is at 25°C.

Medium	Density [g/cm^3]	Speed of Sound [m/s]
PBS	1.01	1505
Histopaque 25 %	1.02153	1509
Histopaque 50 %	1.03786	1512
Histopaque 75 %	1.05743	1511
Histopaque 100 %	1.07501	1515

Table 3.4: The result of the calculated density and compressibility of the BT20 and BT549 cell line.

Cell line	Solution	Density[kg/m^3]	compressibility[1/TPa]
BT20	1	-828.2	4106.1
	2	-104.1	-1443.8
BT549	1	-1115.7	2706.7
	2	229.6	-271.2

The density and compressibility are negative which is nonphysical and can not be used for the calculation for the optimized buffer medium for the separation experiment. The problem seems to be the contrast factor being much lower than expected. This could be due to cells having large variation in sizes. To avoid using the radius of the cells as a parameter for the calculation, we decided to measure the acoustic mobility of the cells instead and compare the mobility ratio of the cells in different buffer mediums. The acoustic mobility is defined as,

$$Acoustic\ mobility = \phi a^2 \tag{3.1}$$

and by using the ratio of acoustic mobilities between reference particles and cells,

$$\frac{\alpha_p}{\alpha_c} = \frac{\phi_p a_p^2}{\phi_c a_c^2} \tag{3.2}$$

we avoid the uncertainty introduced by the measured size of the cells which has a large size distributions used in the parameter a_o^2 in Equation 2.5. The buffer media in which the measurement for the acoustic mobility was performed in is shown in table 3.3. The equation for the compressiblity of two immisible fluids has been derived by Leibacher [43] which is:

$$\kappa = \frac{(V_1\kappa_1 + V_2\kappa_2)}{V_{tot}} \tag{3.3}$$

where κ is the compressibility of the mixture, V_1, V_2 and κ_1, κ_2 are the volume and compressibility of the two fluids respectively and V_{tot} is the total volume of the mixture. The mixture follows the mixing rule and according to equation 3.3, the compressibility of the mixture should be linear with respect to the volume proportion of the two liquids.The theory that is presented by Leibacher agrees well with our measurements presented in figure 3.12, despite we did the measurements on miscible fluids.

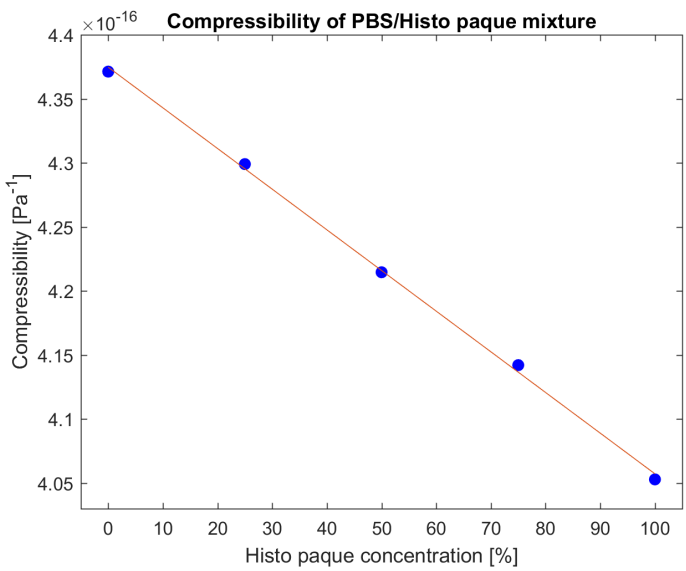

Figure 3.12: Compressibility of the PBS and Histopaque mixture where we have a linear relation between the compressibility and the ratio of the mixture.

With the data from table 3.3 and the measured velocities of the cells, the acoustic mobility of the cels MCF7 and BT20 was calculated and plotted in figure 3.13

and table 3.5. The acoustic mobility is overlapping for the MCF7 and BT20 for concentrations of 25 % and up and has the biggest ratio in PBS with no Histopaque addition as seen in figure 3.14 and 3.6. This indicates that the most optimum buffer solution for separation out of the ones that have been tried is PBS. One reason for the large standard deviation could be that some of the measured cells are in clusters which will have larger volume compared to the single cells.

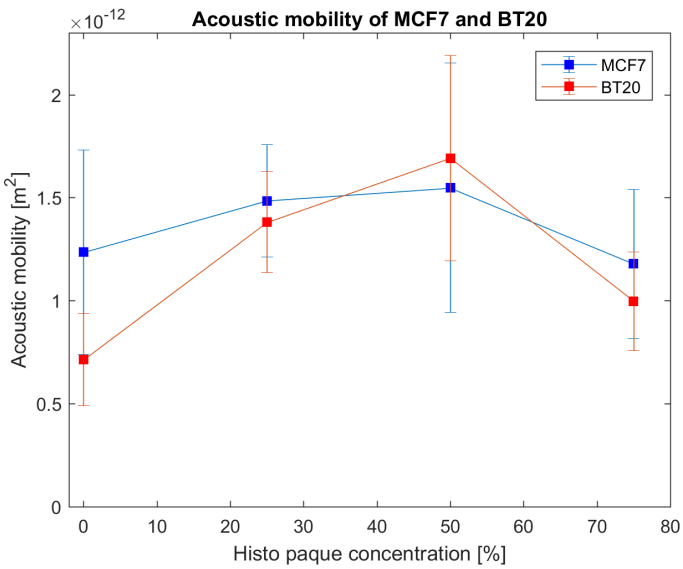

Figure 3.13: The acoustic mobility of MCF7 and BT20 depending on the Histopaque concentration in PBS/Histopaque mixture. The largest difference in the acoustic mobility is seen in PBS, while the PBS/Histopaque mixture showed only minor differences. Furthermore, the large standard deviation which overlaps the data points makes the data unreliable.

Table 3.5: The values of the acoustic mobility measurements which is plotted in figure 3.13.

Histopaque concentration [%]	0	25	50	75
BT20 Mean [m^2]	7.1356e-13	1.3813e-12	1.692e-12	9.9718e-13
BT20 STD [m^2]	2.2304e-13	2.4579e-13	4.984e-13	2.3911e-13
MCF7 Mean [m^2]	1.2351e-12	1.4843e-12	1.5481e-12	1.1792e-12
MCF7 STD [m^2]	4.9651e-13	2.7239e-13	6.0479e-13	3.6176e-13

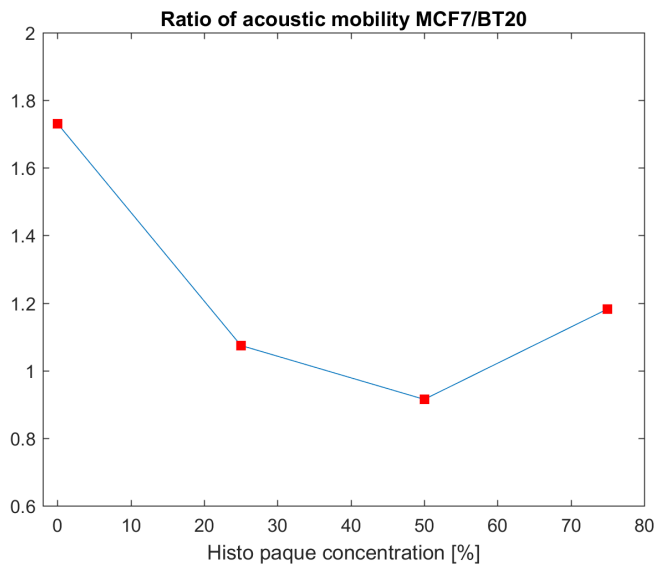

Figure 3.14: Ratio of acoustic mobility between MCF7 and BT20. PBS was shown to give the highest difference in acoustic mobility between the two cell types.

Table 3.6: The values of the acousitc mobility ratio between MCF7 and BT20 which is plotted in figure 3.14.

HistoPaque concentration [%]	0	25	50	75
Ratio of mobility	1.7309	1.0746	0.9150	1.1825

3.5 Separation of tumor cells with Acoustophoresis

The cell suspension with 6.67· 10^5 cells/mL consisting of 1 mL PBS, 1 mL 1· 10^6/mL MCF7 suspension and 1 mL 1· 10^6/mL BT20 suspension was first prepared and analysed with flow cytometry as seen in figure 3.15. The calculation for the separation efficiency and separation purity was done using the values from the event within the MCF7 positive and BT20 positive gating shown in figure 3.15.

According to the results of the mobility measurement experiments, the biggest difference in acoustic mobility between MCF7 and BT20 was achieved in PBS without any addition of Histopaque. Therefore, the separation experiment was done in PBS and the result is shown in table 3.7 and table 3.8.

Table 3.7: The number of positive cells present in the center and side outlet after the separation with different focus voltages.

Focus voltage [V]	3.6	4.2	4.8	5.4	6.0	6.6	7.2
MCF7 Center outlet	4	3	157	56	208	201	550
MCF7 Side outlet	989	1065	746	311	134	8	2
BT20 Center outlet	10	11	144	77	426	358	827
BT20 Side outlet	1124	1176	1025	420	280	116	124

Table 3.8: The separation efficiency and purity of MCF7 and BT20 mixture for different focusing voltage.

Focusing Voltage [V]	3.6	4.2	4.8	5.4	6.0	6.6	7.2
MCF7 Separation Efficiency[%]	0.4	0.3	17.3	15.3	60.8	96.2	99.6
MCF7 Separtion Purity[%]	28.6	21.4	52.2	42.4	32.8	36.0	39.9
BT20 Separation Efficiency[%]	0.9	0.9	12.3	15.3	60.3	75.5	87.0
BT20 Separation Purity[%]	71.4	78.6	47.8	57.5	67.2	64.0	60.1

The separation efficiency is overlapping for the entire range of voltages that has been tested for the two cell types which leads to difficulty in separation, also seen

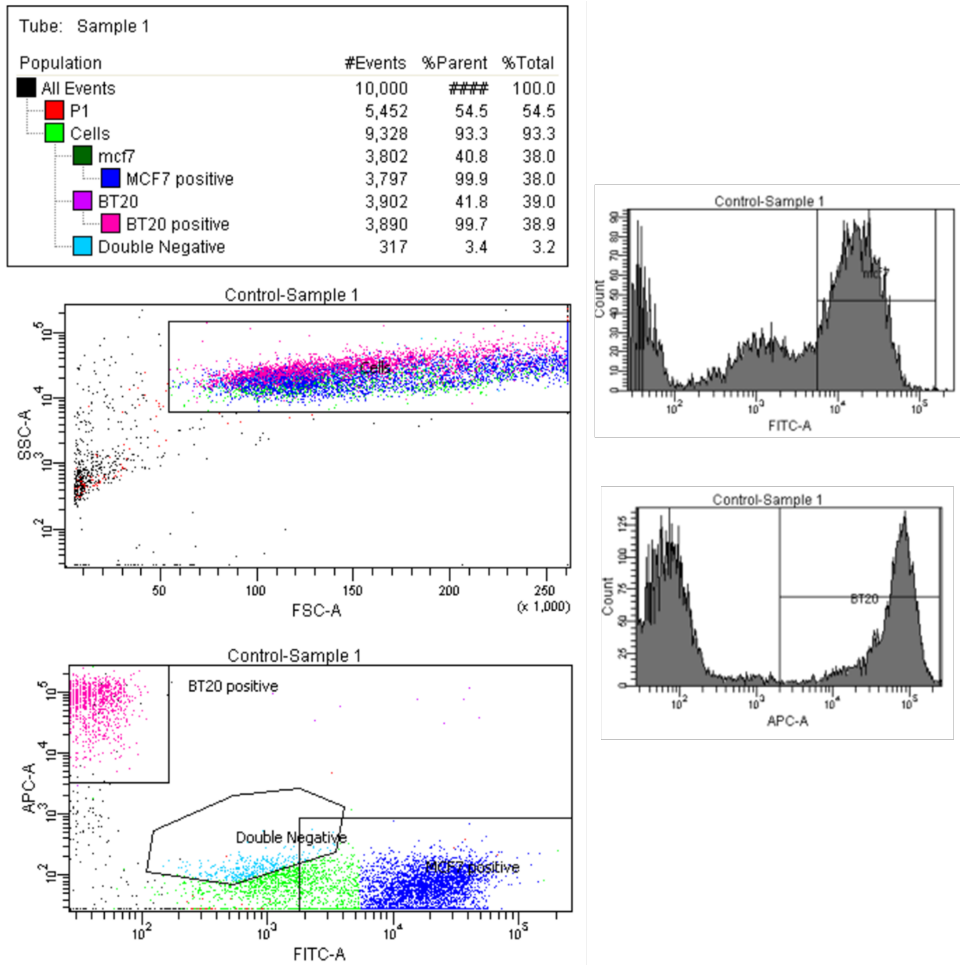

Figure 3.15: The mixture of cells that was separated with the acoustophoresis setup. All the events within the gating Cells is gated for MCF7 and BT20 and for their staining.

in figure 3.16. In figure 3.16(a), the size variation in the MCF7 population appears as multiple lines in the channel. This distribution is also present in the BT20 population as seen in figure 3.16(b). The streams of MCF7 and BT20 is overlapping and therefore, we could not get a good separation.

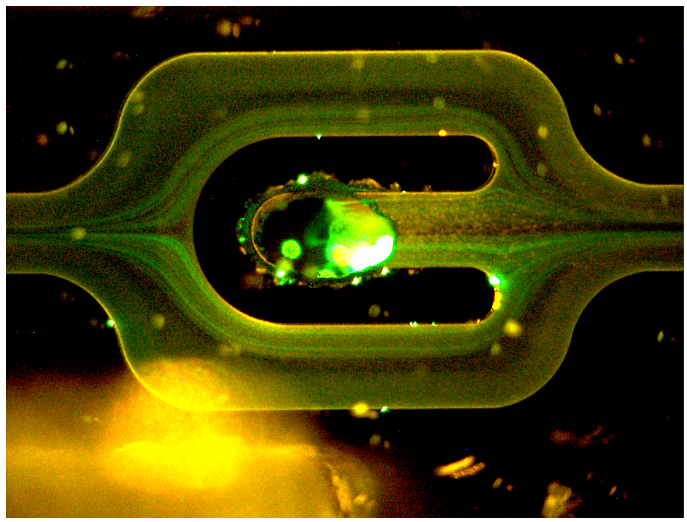

(a)

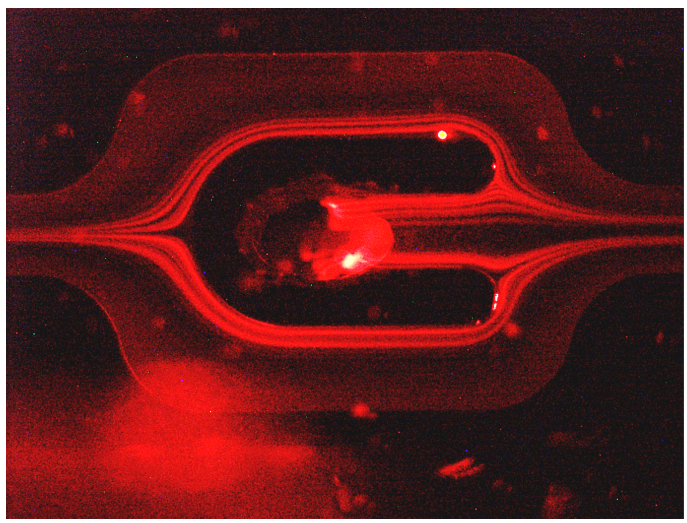

(b)

Figure 3.16: Separation channel with mixture of MCF7(green) and BT20(red) suspended in PBS. The amplitude of the focusing voltage is 4.8 V. The images are taken by changing the filter while ongoing separation. Both the MCF7 and BT20 cells are focused in multiple lines due to it having size distributions.

Chapter 4

Conclusions and Outlook

New ways to characterize and extract the different cancer cells might prove to be helpful towards research of breast cancer treatment. As of the cell dissociation of frozen patient samples, it seems to be a challenging task to obtain live cells and would require a more refined method for cryo-preserving these samples. Unfortunately, there was not enough time and resources to test the dissociation on fresh tissue to be able to establish and refine the protocol for the tumor dissociation. There are several challenges such as transportation and logistics to get the tissue samples delivered without minimal cell death and to then conduct the experiment on. However, If this could be made possible, it would create a potential for us to gain new knowledge which could further our understanding and treatment possibilities. As for the separation of breast cancer cell lines, we could establish that Histopaque that was used was not suitable for the separation of MCF7 and BT20. The mobility ratio between the cells in PBS/Histopaque mixture were too similar to be used as the buffer. Unfortunately, there were not enough time to try other different density media which could have given more promising results. In future experiments, density media with wider range of densities and compressibility could be tested which hopefully enable separation of these cells.

Chapter 5

Populärvetenskaplig sammanfattning

Hur rör sig bröstcancerceller i det akustiska fältet?

Bröstcancer är en av dom vanligaste åkommorna som drabbar kvinnor i världen. Sjukdomens stora variation och komplexitet medför att behandlingsstrategier och hur patienten reagerar till behandlingen varierar stort mellan individerna. Det finns fortfarande mycket forskning kvar att utföra för att finna effektiva metoder för diagnostik och behandling av dom olika cancerformerna. Inom det biomedicinska fältet finns det stort värde i metoder som används för att separera ut celler och partiklar från en lösning. Om det inte går att isolera cellen av intresse, kan andra celler och ämnen i provet bidra med felaktiga data vilket kan leda till att felaktiga slutsatser dras. Mikrofluidik är ett fält som har väckt stort intresse inom biomedicinsk tillämpning. Detta på grund av dess många fördelar som till exempel, minskad materialkostnad eftersom man jobbar med små volymer och laminärt flöde där flödet är förutsägbart och kan därmed utföra bra simuleringar. I denna rapport använder vi oss av mikrofluidiktekniken som kallas akustofores för att separera bröstcancerceller. Akustoforestekniken använder ultraljud som appliceras på mikrofluidikchip med små vätskefyllda kanaler. Kanalerna har typiskt sätt bredd och höjd i mikrometer och längd i centimeterskalan. Måtten på kanalen är specifikt valda för att ge upphov till stående vågor inuti kanalen när ultraljudvågorna appliceras. Objekten som befinner sig i det akustiska fältet utsätts för akustiska krafter, vilket interagerar och flyttar på partiklar och celler blandade i vätskan inne i mikrofluidikkanalen. Styrkan och riktningen hos den akustiska kraften beror på storleken på partiklarna och den relativa densiteten och kompressabiliteten mellan

vätskan och objekten blandade i vätskan. Tecknet och storleken på den akustiska kontrastfaktorn ϕ som beror på den relativa densiteten och kompressabiliteten mellan vätskan och objekten indikerar om hur snabbt objektet kommer att flytta sig mot noderna eller antinoderna hos den stående vågen. I detta projekt försökte vi att separera ut bröstcancerceller från nedfrusna biopsiprover från patienter med hjälp av akustofores. Först fick patientproverna genomgå preparationssteg där de först analyserades kvalitativt om de innehöll tillräckligt med cancerceller för att utföra experimenten på. Detta gjordes genom att 10 mikrometer tunna skivor av frusen vävnad skars av och analyserades kvalitativt genom Hematoxylin och Eosin infärgning (H&E-infärgning) som färgar in cellkärnor och stromaceller. Sedan extraherades cellerna från tumörvävnaden genom celldissociering där vävnaderna bröts ned både enzymatiskt och mekaniskt till en cellsuspension vilket skulle undergå separation med akustofores. Tyvärr uppstod ett problem här vilket innebar att vi inte kunde utföra några separationsexperiment med patientproverna. Detta var på grund av att vi inte kunde få ut tillräckligt med levande celler för experimenten vilket berodde på flera orsaker. Första är att vi var inte tillräckligt erfarna för att utföra celldissociationen då det ingick många steg av preparation av prover, kontrollceller och flera steg av infärgning. Den andra anledning vilket var den mest avgörande var att patientproverna förmodligen blev förstörda när de frystes ner utan några strategier för att förhindra celldöd vid frysning. Eftersom vi inte kunde få ut några celler behövde vi ändra på målsättningen av projektet. Därmed fortsattes experimenten på cellinjer av bröstcancerceller där cellinjerna MCF7, BT20 och BT549 skulle separeras från varandra med akustofores. Målet blev nu att optimera separationen av cellerna från varandra genom att designa en buffertlösning med densitet och kompressabilitet som ger bästa separation. Först gjordes mätningar för att ta reda på kontrastfaktorn hos cellerna i Phosphate buffered saline (PBS) och en blandning av PBS och ett densitetmedium som kallas Histopaque. Utifrån mätningarna av kontrastfaktorn och storleksmätningar av cellerna kunde vi ta reda på densiteten och kontrastfaktorn av cellerna. Tyvärr visade sig att kontrastfaktorn som vi mätte upp var felaktiga och orimliga och därmed kunde vi inte få ut värden på densiteten och kompressabiliteten hos cellerna. Detta är förmodligen på grund av att cellerna har en stor distribution i dess storlek inom populationen och det ger stor osäkerhet då kontrastfaktorn är proportionellt med radien i kvadrat. För att undvika detta problem mättes i stället förhållandet mellan den akustiska mobiliteten hos cellerna. Det visade sig då att PBS skulle ge den bästa separationen. Vid försök att separera cellerna lyckades vi inte få en optimerad separation trots allt. Våra slutsatser som

vi kan dra från projektet är följande: Det behövs en bättre strategi för att frysa ner och förvara patientproverna om inte färsk vävnad används för experimenten. För att separera cellerna behöver vi testa fler densitetsmedia för att se om vi kan hitta ett media och koncentration som har densitet och kompressabilitet som är mer lämpad för att separera bröstcancercellerna från varandra.

List of Figures

List of Tables

Nomenclature

η	Dynamic viscosity
κ_m	Compressibility of the medium
κ_p	Compressibility of the particle
μ	Viscosity of the fluid
v_y	Velocity of suspended particle in the acoustic field
ϕ	Acoustic contrast factor
ρ_c	Density of the cell
ρ_m	Density of the medium
ρ_p	Density of the particle
a	Radius of the particle
D	Diffusion coefficient
d	Center to center distance between two particles
E_{ac}	Acoustic energy density
F_{drag}	Stokes drag
F_{rad}	Acoustic radiation force
F_{sec}	Secondary acoustic radiation force
k_y	Wave number

L	Characteristic length of the system
p	Pressure
p_1	First order pressure field p_a
Pe	Péclet number
Re	Reynolds number
u	Average flow speed of the fluid

Bibliography

[1] H. Ellis and V. Mahadevan, "Anatomy and physiology of the breast," *Surgery (Oxford)*, vol. 31, no. 1, pp. 11–14, 2013.

[2] R. A. Lawrence, R. A. Lawrence, and R. M. Lawrence, "2 - anatomy of the breast," in *Breastfeeding (Ninth Edition)*, pp. 38–57, Philadelphia: Elsevier, 2022.

[3] C. Desantis, J. Ma, M. Gaudet, L. Newman, K. Miller, G. Sauer, A. Jemal, A. Siegel, and R, "Breast cancer statistics," *CA Cancer J Clin*, vol. 69, pp. 438–451, 10 2019.

[4] A. Basu, G. Ramamoorthi, Y. Jia, J. Faughn, D. Wiener, S. Awshah, K. Kodumudi, and B. J. Czerniecki, "Chapter six - immunotherapy in breast cancer: Current status and future directions," in *Immunotherapy of Cancer* (X.-Y. Wang and P. B. Fisher, eds.), vol. 143 of *Advances in Cancer Research*, pp. 295–349, Academic Press, 2019.

[5] R. B. Schwab, M. Koehler, S. M. Ali, and B. W. Murray, "Genomic profiling and treatment of her2+, er+, pgr+ "triple positive" breast cancer: A case report and literature review," *Cancer Treatment and Research Communications*, vol. 9, pp. 27–31, 2016.

[6] S. Mashhadizadeh, M. Tavangar, A. Fallahiyan Javani, M. D. Rahimian, M. Azadeh, H. Tabatabaeian, and K. Ghaedi, "Pgr and tug1 overexpression: A putative diagnostic biomarker in breast cancer patients," *Gene Reports*, vol. 21, p. 100791, 2020.

[7] S. Mani, G. Swargiary, S. Gulati, S. Gupta, and D. Jindal, "Molecular docking and admet studies to predict the anti-breast cancer effect of aloin by targeting estrogen and progesterone receptors," *Materials Today: Proceedings*, 2021.

[8] T. E. Hickey, L. A. Selth, K. M. Chia, G. Laven-Law, H. H. Milioli, D. Roden, S. Jindal, M. Hui, J. Finlay-Schultz, E. Ebrahimie, S. N. Birrell, S. Stelloo, R. Iggo, S. Alexandrou, C. E. Caldon, T. M. Abdel-Fatah, I. O. Ellis, W. Zwart, C. Palmieri, C. A. Sartorius, A. Swarbrick, E. Lim, J. S. Carroll, and W. D. Tilley, "The androgen receptor is a tumor suppressor in estrogen receptor-positive breast cancer," *Nature Medicine*, vol. 27, no. 2, pp. 310–320, 2021.

[9] I. Migliaccio, M. Bonechi, A. McCartney, C. Guarducci, M. Benelli, L. Biganzoli, A. Di Leo, and L. Malorni, "Cdk4/6 inhibitors: A focus on biomarkers of response and post-treatment therapeutic strategies in hormone receptor-positive her2-negative breast cancer," *Cancer Treatment Reviews*, vol. 93, p. 102136, 2021.

[10] D. Zhou, Y. Wu, K. Jiang, F. Xu, R. Hong, and S. Wang, "Identification of a risk prediction model for clinical prognosis in her2 positive breast cancer patients," *Genomics*, vol. 113, no. 6, pp. 4088–4097, 2021.

[11] K. Liang, Y. Lu, W. Jin, K. K. Ang, L. Milas, and Z. Fan, "Sensitization of breast cancer cells to radiation by trastuzumab," *Molecular Cancer Therapeutics*, vol. 2, no. 11, pp. 1113–1120, 2003.

[12] M. G. Cesca, L. Vian, S. Cristóvão-Ferreira, N. Pondé, and E. de Azambuja, "Her2-positive advanced breast cancer treatment in 2020," *Cancer Treatment Reviews*, vol. 88, p. 102033, 2020.

[13] S.-Y. Park, J.-H. Choi, and J.-S. Nam, "Targeting cancer stem cells in triple-negative breast cancer.," *Cancers*, vol. 11, 7 2019.

[14] W. D. Foulkes, I. E. Smith, and J. S. Reis-Filho, "Triple-negative breast cancer," *New England Journal of Medicine*, vol. 363, no. 20, pp. 1938–1948, 2010. PMID: 21067385.

[15] R. Dent, M. Trudeau, K. I. Pritchard, W. M. Hanna, H. K. Kahn, C. A. Sawka, L. A. Lickley, E. Rawlinson, P. Sun, and S. A. Narod, "Triple-negative breast cancer: Clinical features and patterns of recurrence," *Clinical Cancer Research*, vol. 13, no. 15, pp. 4429–4434, 2007.

[16] R. Jones and J. Ocen, "Cytotoxic chemotherapy: clinical aspects," *Medicine*, vol. 48, no. 2, pp. 97–102, 2020.

[17] X. Bai, J. Ni, J. Beretov, P. Graham, and Y. Li, "Immunotherapy for triple-negative breast cancer: A molecular insight into the microenvironment, treatment, and resistance," *Journal of the National Cancer Center*, vol. 1, no. 3, pp. 75–87, 2021.

[18] A. C. Degnim, R. D. Brahmbhatt, D. C. Radisky, T. L. Hoskin, M. Stallings-Mann, M. Laudenschlager, A. Mansfield, M. H. Frost, L. Murphy, K. Knutson, and D. W. Visscher, "Immune cell quantitation in normal breast tissue lobules with and without lobulitis," *Breast Cancer Research and Treatment*, vol. 144, no. 3, pp. 539–549, 2014.

[19] Y. Asano, S. Kashiwagi, W. Goto, K. Kurata, S. Noda, T. Takashima, N. Onoda, S. Tanaka, M. Ohsawa, and K. Hirakawa, "Tumour-infiltrating cd8 to foxp3 lymphocyte ratio in predicting treatment responses to neoadjuvant chemotherapy of aggressive breast cancer," *Br J Surg*, vol. 103, pp. 845–854, Mar. 2016.

[20] K. Wang, T. Shen, G. P. Siegal, and S. Wei, "The cd4/cd8 ratio of tumor-infiltrating lymphocytes at the tumor-host interface has prognostic value in triple-negative breast cancer," *Human Pathology*, vol. 69, pp. 110–117, 2017.

[21] H. Y. Wang, D. A. Lee, G. Peng, Z. Guo, Y. Li, Y. Kiniwa, E. M. Shevach, and R.-F. Wang, "Tumor-specific human cd4+ regulatory t cells and their ligands: Implications for immunotherapy," *Immunity*, vol. 20, no. 1, pp. 107–118, 2004.

[22] J. Geginat, M. Paroni, S. Maglie, J. S. Alfen, I. Kastirr, P. Gruarin, M. De Simone, M. Pagani, and S. Abrignani, "Plasticity of human cd4 t cell subsets," *Frontiers in Immunology*, vol. 5, p. 630, 2014.

[23] M. W. Teng, S. F. Ngiow, B. von Scheidt, N. McLaughlin, T. Sparwasser, and M. J. Smyth, "Conditional regulatory t-cell depletion releases adaptive immunity preventing carcinogenesis and suppressing established tumor growth," *Cancer Research*, vol. 70, no. 20, pp. 7800–7809, 2010.

[24] S. Taefehshokr, A. Parhizkar, S. Hayati, M. Mousapour, A. Mahmoudpour, L. Eleid, D. Rahmanpour, S. Fattahi, H. Shabani, and N. Taefehshokr, "Cancer immunotherapy: Challenges and limitations," *Pathology - Research and Practice*, p. 153723, 2021.

[25] A. Folch, "Microfluidics," in *Introduction to BioMEMS*, ch. 3, Boca Raton: CRC Press Taylor & Francis group, 1 ed., 2012.

[26] R. Barnkob, *Physics of microparticle acoustophoresis: Bridging theory and experiment.* PhD thesis, 2012.

[27] F. Petersson, L. Åberg, A.-M. Swärd-Nilsson, and T. Laurell, "Free flow acoustophoresis: Microfluidic-based mode of particle and cell separation," *Anal. Chem.*, vol. 79, pp. 5117–5123, July 2007.

[28] P. Augustsson and T. Laurell, "Acoustofluidics 11: Affinity specific extraction and sample decomplexing using continuous flow acoustophoresis," *Lab Chip*, vol. 12, pp. 1742–1752, 2012.

[29] A. Lenshof, C. Magnusson, and T. Laurell, "Acoustofluidics 8: Applications of acoustophoresis in continuous flow microsystems," *Lab Chip*, vol. 12, pp. 1210–1223, 2012.

[30] H. Bruus, "Acoustofluidics 7: The acoustic radiation force on small particles," *Lab Chip*, vol. 12, pp. 1014–1021, 2012.

[31] A. Lenshof, C. Johannesson, M. Evander, J. Nilsson, and T. Laurell, "Acoustic cell manipulation," in *Microtechnology for Cell Manipulation and Sorting* (W. Lee, P. Tseng, and D. Di Carlo, eds.), pp. 129–173, Cham: Springer International Publishing, 2017.

[32] M. Gröschl, "Ultrasonic separation of suspended particles - part i: Fundamentals," 1998.

[33] S. S. Sadhal, "Acoustofluidics 13: Analysis of acoustic streaming by perturbation methods," *Lab Chip*, vol. 12, pp. 2292–2300, 2012.

[34] A. Lenshof, M. Evander, T. Laurell, and J. Nilsson, "Acoustofluidics 5: Building microfluidic acoustic resonators," *Lab Chip*, vol. 12, pp. 684–695, 2012.

[35] P. Geng, C. Li, X. Ji, and S. Dong, "Numerical simulation of microfluidic mixing by ultrasonic-induced acoustic streaming," *Journal of Dispersion Science and Technology*, vol. 42, no. 11, pp. 1623–1633, 2021.

[36] H.-P. Sinn and H. Kreipe, "A brief overview of the who classification of breast tumors, 4th edition, focusing on issues and updates from the 3rd edition," 2013.

[37] M. Lacroix and G. Leclercq, "Relevance of breast cancer cell lines as models for breast tumours: An update," *Breast Cancer Research and Treatment*, vol. 83, no. 3, pp. 249–289, 2004.

[38] S. V. Pande and J. F. Mead, "Inhibition of enzyme activities by free fatty acids," *Journal of Biological Chemistry*, vol. 243, no. 23, pp. 6180–6185, 1968.

[39] J. E. Fletcher, A. A. Spector, and J. D. Ashbrook, "Analysis of long-chain free fatty acid binding to bovine serum albumin by determination of stepwise equilibrium constants," *Biochemistry*, vol. 10, no. 17, pp. 3229–3232, 1971. PMID: 5165844.

[40] ThermoFisher, *CalceinAM User guide*. Waltham: ThermoFisher, 2020.

[41] A. Lenshof, *Lab preparation for the Acoustophoresis lab 2021*. Lund: Lund University, 2021.

[42] Augustsson, Per, *On microchannel acoustophoresis - Experimental considerations and life science applications*. PhD thesis, Lund University, 2011.

[43] I. Leibacher, W. Dietze, P. Hahn, J. Wang, S. Schmitt, and J. Dual, "Acoustophoresis of hollow and core-shell particles in two-dimensional resonance modes," *Microfluidics and Nanofluidics*, vol. 16, no. 3, pp. 513–524, 2014.